Applied Catalysis B: Environmental 214 (2017) 1–14

Contents lists available at ScienceDirect

Applied Catalysis B: Environmental

journal homepage: www.elsevier.com/locate/apcatb

High hexitols selectivity in cellulose hydrolytic hydrogenation over platinum (Pt) vs. ruthenium (Ru) catalysts supported on micro/mesoporous carbon

P.A. Lazaridis[a], S.A. Karakoulia[b], C. Teodorescu[c], N. Apostol[c], D. Macovei[c], A. Panteli[a], A. Delimitis[b], S.M. Coman[d,**], V.I. Parvulescu[d,**], K.S. Triantafyllidis[a,b,*]

[a] Department of Chemistry, Aristotle University of Thessaloniki, GR-54124 Thessaloniki, Greece
[b] Chemical Process & Energy Resources Institute, CERTH, GR-57001 Thessaloniki, Greece
[c] National Institute of Materials Physics, Atomistilor 105b, 077125 Magurele, Ilfov, Romania
[d] Department of Organic Chemistry, Biochemistry and Catalysis, Faculty of Chemistry, University of Bucharest, Regina Elisabeta Blvd., No. 4-12, Bucharest 030016, Romania

ARTICLE INFO

Article history:
Received 24 January 2017
Received in revised form 4 May 2017
Accepted 9 May 2017
Available online 10 May 2017

Keywords:
Cellulose
Hydrolytic hydrogenation
Sugar alcohols
Platinum vs. ruthenium
Micro/mesoporous carbon

ABSTRACT

The "one-pot" hydrolyltic hydrogenation of cellulose towards C2-C6 sugar alcohols has been recognized as one of the most promising biomass valorization routes for the production of high added-value chemicals. In this work, we studied the performance of Ru and Pt catalysts supported on micro/mesoporous activated carbon, in the hydrolytic hydrogenation of microcrystalline and ball-milled cellulose, in neat water, at 180 °C and at relatively low hydrogen pressure of 2 MPa. The impact of metal loading (1–5 wt.%), metal reduction method (H_2 at 350 °C or $NaBH_4$) and acidification (sulfonation) of the AC support on cellulose conversion and selectivity to the various products were systematically addressed. It was shown that Pt is significantly more selective towards hexitols (sorbitol and mannitol) compared to Ru, in glucose-rich reaction media, such as those offered by the easily hydrolyzed ball-milled cellulose. For example, the 5wt%Pt/AC-SO_3H catalyst afforded hexitols yield of 69.5 wt.% (at 96.1% conversion) compared to 10.9 wt.% (at 95.2% wt.% conversion) obtained by the corresponding Ru catalyst, the latter being also selective towards glycerol and propane-1,2-diol (propylene glycol). A relatively moderate metal loading, such as in 3 wt.%Ru/AC-SO_3H, was more favorable for hexitols production (44.5 wt.% yield, at 94.8 wt.% conversion) with Ru catalysts. These results were also verified by glucose hydrogenation experiments that were conducted at the same experimental conditions. Both Pt and Ru exhibited relatively high glucose hydrogenation activity towards hexitols, versus retro-aldol reactions that lead directly to smaller C2–C4 compounds, while the difference in the final product yields between the two metals was attributed to the higher hexitols hydrogenolysis (C—C cleavage) reactivity of Ru. HRTEM data showed the formation of metallic crystalline Pt and Ru nanoparticles (≤4 nm, depending on loading) as well as of amorphous oxygen-rich $M(O)_x^{\delta+}$ phases, which were also confirmed by the XPS data. The presence of these phases which may be a source of acidity, as well as the bacisity of the parent AC used in this study, were mainly responsible for inducing isomerization, retro-aldol and dehydration reactions leading eventually to increased glycerol and propylene glycol selectivity, as was observed for both low-metal catalysts, i.e. 1 wt.% Pt or Ru/AC.

1. Introduction

Carbohydrates being the primary building block components of lignocellulosic biomass have the potential to supplement petroleum-derived hydrocarbons and other high-added value chemicals. In a general biorefinery concept, lignocellulosic biomass is initially fractionated to its constitutive bio-polymers, i.e. hemicellulose, cellulose and lignin, which can be further selectively

* Corresponding author at: Department of Chemistry, Aristotle University of Thessaloniki, GR-54124 Thessaloniki, Greece.
** Corresponding authors.
E-mail addresses: simona.coman@g.unibuc.ro (S.M. Coman), vasile.parvulescu@chimie.unibuc.ro (V.I. Parvulescu), ktrianta@chem.auth.gr (K.S. Triantafyllidis).

http://dx.doi.org/10.1016/j.apcatb.2017.05.031
0926-3373/

transformed to molecules with multiple functional groups and varying potential applications, either as platform chemicals or as fuel components [1–4]. Thereby, the investigation and discovery of novel and efficient pathways for the conversion of lignocellulosic biomass into chemicals are among the biggest challenges in the field of catalysis, in general, and heterogeneous catalysis, in particular. Although research in this area is very intense and new transformation routes and catalytic materials have been already proposed, the specific properties of biomass (i.e. recalcitrant nature of "crystalline" cellulose, high reactivity of intermediate products, etc.) impose difficulties that still need to be overcome for the development of sustainable and scalable industrial processes.

With regard to cellulose valorization, the first step is its hydrolysis to glucose monomers that can then be selectively converted to a wide range of platform chemicals. Cellulose hydrolysis can be performed by the use of mineral acids or enzymes, while more recently, heterogeneous catalytic systems have been proposed in order to overcome the drawbacks of the first two technologies [5,6]. The solid acid catalysts that have been studied for the hydrolysis of cellulose include amongst others, functionalized/acidified polymers and carbon- or silica-based materials [5–11]. An alternative promising approach that has been developed in the last years is the combination of cellulose hydrolysis with hydrogenation/hydrogenolysis of the derived glucose, in "one-pot" process that can lead to the selective formation of valuable sugar alcohols (i.e., sorbitol, erythritol) or smaller polyols and glycols (propylene and ethylene glycol, glycerol, etc.) which may find numerous applications in the food, pharmaceutical, polymer and fuel industry [12–18].

The so-called hydrolytic hydrogenation of cellulose requires bifunctional (hydrogenating metals supported on acidic materials) solid catalysts [18–26] or a mineral acid [18,27–29] or heteropoly acid [18,30,31] in combination with a solid hydrogenation catalyst. Many studies have discussed the in situ formation of protons via the dissociative adsorption of molecular hydrogen on the hydrogenating metal (i.e. Ru, Pt) and the reversible spillover of atomic H species to the support surface, as a source of acidity for the initial step of cellulose hydrolysis [21,24,25]. Indeed, kinetic studies indicated that the hydrogenating metals can promote both hydrolysis and hydrogenation steps [22,32]. At relatively high reaction temperatures (ca. >200 °C), the acidity needed for the initial cellulose hydrolysis may also be provided by the hydronium ions generated under the subcritical water conditions applied [26,33]. It was found, for instance, that Ru supported on mesoporous carbon (i.e., CMK-3) catalyzes the hydrolysis of cellulose to glucose via formation of oligosaccharides in hot compressed water without adding any acid catalysts [34,35]. In addition, Ru & Pt/CMK-3 catalysts have also been tested in cellulose hydrogenation reactions using 2-propanol as a source of hydrogen (transfer hydrogenation). Both metal catalysts were active in cellulose conversion, but Ru/CMK-3 gave relatively higher yields of sugar alcohols compared to the respective Pt catalyst [36].

In the absence of mineral acids or heteropoly acids, the use of acidic supports is generally necessary for enhancing the hydrolysis of cellulose, regardless the promotional effect of hydrogenation metals, such as Ru, Pt, Pd, etc., as discussed above. The most studied acidic supports comprise carbon based materials which have been appropriately pre-treated to increase their surface acidity by $-SO_3H$, –COOH or –OH groups (i.e., different types of activated carbons [37] or carbon nanotubes [19,38]), metal oxides with or without modification (i.e. Al_2O_3 [19,21,32,39], SiO_2 [19,40], SiO_2-Al_2O_3 [25], sulfonated silica/carbon [41]) and zeolites (i.e., ZSM-5 [42,43], *meso*-ZSM-5 [44], Beta [45], USY [21,28,43], Mordenite [28]). Although zeolites can offer their inherent acidity for the enhancement of cellulose hydrolysis their stability in hot liquid water conditions is under discussion [28,46]. However, stable catalytic systems using zeolite HY as support in glucose hydrogenation to sorbitol have been more recently reported [47]. In addition, hexitols could be obtained with nearly quantitative yields for multiple consecutive runs using Ru/H-USY zeolites [48,49]. On the other hand, carbon based materials are generally more stable under these conditions [23,50] and even sulfonated carbon catalysts have exhibited stable performance in cellulose hydrolytic hydrogenation [19,37]. Due to their increased hydrothermal stability, high surface area, varying micro/mesoporosity and rich surface functionalization chemistry, activated carbons and other carbon nanostructures have been used as supports in various hydrolysis-hydrogenation processes, such as glucose hydrogenation towards sugar alcohols [18,51–54], hemicellulose (arabinogalactan, arabinoxylan) hydrolytic hydrogenation [55] and hemicellulose sugars (arabinose, galactose, xylitol) hydrogenation [56,57]. With regard to the hydrogenating metal, the ones that have been studied more are Ni, Ru, Pt, Pd, Ir and Rh, as already mentioned above [4,11,14,18,19,58]. The particle size of the metals has been also shown to affect activity and product selectivity. In a relevant study, the Ru/CNT catalysts with larger mean size of Ru nanoparticles (≥8.7 nm) and higher acidity of the CNTs exhibited better sorbitol yield in the hydrogenation of cellobiose [38].

Cellulose pretreatment prior to hydrolytic hydrogenation has been also shown to significantly affect reactivity and product selectivity. The reduction of cellulose crystallinity and particle size by ball-milling can induce increased conversion and higher hexitols yields due to enhanced hydrolysis rates, compared to untreated microcrystalline cellulose [22,26,28,40,59–61]. Partial deconstruction of cellulose prior to the hydrogenolysis has also been attempted by its pretreatment with aqueous H_3PO_4 solutions at different temperatures [19]. A further improvement in conversion and selectivity can be achieved by mechanocatalytic pretreatment of cellulose where cellulose is impregnated with small amounts of mineral acids, i.e. H_2SO_4 or HCl, prior to ball-milling [50,62].

Based on the current progress in the field, the present study aims to a systematic investigation of the performance of supported noble metals (i.e., Pt and Ru) on activated carbon (AC) in the hydrolytic hydrogenation of cellulose to sugar alcohols and smaller glycols. The impact of catalyst preparation parameters, such as metal concentration, metal reduction method and acidification of the AC support on cellulose conversion and selectivity to the various products were systematically addressed. A high surface area activated carbon with enhanced mesoporosity was also chosen in order to enhance the dispersion of the metal nanoparticles and facilitate diffusion of reactants and products. Relatively mild reaction conditions were applied (i.e. 2 MPa H_2 pressure and 180 °C). Glucose hydrogenation experiments under the same conditions were also performed in order to investigate the reaction mechanism and rationalize the observed products in cellulose hydrolytic hydrogenation experiments. The effect of cellulose depolymerization by ball-milling and stability of the catalysts were also investigated.

2. Experimental

2.1. Catalyst preparation

The investigated catalysts were based on platinum (Pt) and ruthenium (Ru) metals supported on activated carbon (AC), at nominal loadings of 1, 3, or 5 wt.%. They were prepared by classical wet impregnation method using a micro/mesoporous activated carbon (Norit SAE SUPER, SSA = 1175 m^2/g) and aqeuous solutions of $RuCl_3 \cdot xH_2O$ (Fluka) or hexachloro-platinic (IV) acid hexahydrate (~40%Pt) (Alfa). In a typical preparation of ca. 1 wt.% Ru catalyst, 0.300 mmole of $RuCl_3$ in 20 mL H_2O were added dropwise into a suspension of activated carbon (3 gr) in water (70 mL) under

stirring, and the mixture was further stirred for 22 h at room temperature. After drying in vacuum at 60 °C, the recovered Ru/AC powder was added to 100 mL 0.4 M $NaBH_4$ ethanol solution. The mixture was kept under stirring until the bubble generation ceased (~4 h). The obtained Ru/AC catalyst was separated from the solution by vacuum filtration, followed by thorough washing with deionized water until the pH value of the filtrate was ~7, and was then washed with 50 mL of ethanol. The samples were finally dried at room temperature overnight. The same procedure was applied for the supported Pt catalysts, using hexachloro-platinic (IV) acid hexahydrate (~40%Pt) (Alfa) as metal source. The catalyst samples prepared by the above procedure were denoted as *x%M/AC-B*, were: *x* is the content of the metal (1, 3 or 5 wt.%), *M* is the type of metal (Pt or Ru) and *B* indicates the use of $NaBH_4$ as reductant. The reduction of metals in the impregnated catalysts was also performed in a flow reactor under 100% H_2 flow (50 mL/min) at 350 °C for 1 h (heating rate – 2 °C/min, step-wise heating with 30 min intervals at 150 and 250 °C). The obtained catalyst samples were denoted as *x%M/AC-H*, were *x* is the metal content (1, 3 or 5 wt.%), *M* is the type of metal (Pt or Ru) and *H* indicates the use of H_2 as reductant.

In order to enhance the hydrolysis of cellulose towards glucose, bifunctional catalysts were prepared by supporting the hydrogenating metals Pt or Ru, on acidic carbon which contains surface acidic sulfonic groups. The sulfonated carbon was prepared by mixing the parent activated carbon with c. H_2SO_4 (99.999% purity, 10 mL acid per 1 g carbon) at 80 °C (in oil bath) for 4 h under stirring. After sulfonation, the solid catalyst was recovered by filtration, washed with deionized water until neutral pH of the filtrate and dried overnight at room temperature. The sulfonated carbon was impregnated with aqueous solutions of Pt or Ru, while $NaBH_4$ was used for the in situ reduction of the metals, as described above. The reduction of bifunctional catalysts under hydrogen atmosphere at 350 °C was not possible due to the decomposition of sulfonic groups at these temperatures (≥250 °C). The obtained samples were denoted as *x%M/AC-SO$_3$H*.

2.2. Catalyst characterization

T

he parent activated carbon and supported metal catalysts were characterized with various techniques, such as Inductively Coupled Plasma-Atomic Emission Spectroscopy (ICP-AES), elemental analysis (C,H,S), N_2 sorption at −196 °C, X-ray Diffraction (XRD), X-ray Photoelectron Spectroscopy (XPS), Conventional and High Resolution Transmission Electron Microscopy (TEM-HRTEM) and Boehm titration (determination of total acidity).

The chemical composition (wt.% of Pt and Ru) was determined by ICP-AES using a Plasma 400 (Perkin Elmer) spectrometer, equipped with a Cetac6000AT+ ultrasonic nebulizer. Elemental analysis was performed on a LECO-800 CHN analyzer for C, H and a LECO-S-932 analyzer for S determination.

Powder XRD experiments were conducted on a Shimadzu X-ray 7000 diffractometer using a CuK_α X-ray radiation operating at 45 kV and 100 mA; counts were accumulated in the range of 10–80° 2θ every 0.02° (2θ) with counting time 2 s per step.

Nitrogen adsorption/desorption experiments at −196 °C were performed for the determination of specific surface area (multipoint BET method), total pore volume (at P/Po = 0.99), mircopore area by t-plot analysis and pore size distribution (BJH method using adsorption data or DFT analysis) of the samples which were previously outgassed at 150 °C for 16 h under 5×10^{-9} Torr vacuum, using an Automatic Volumetric Sorption Analyzer (Autosorb-1MP, Quantachrome).

XPS measurements were performed at normal emission using a SSX-100 spectrometer, Model 206 from Surface Science Instrument by using Al K_α monochromated radiation (hν = 1486.7 eV) of an X-ray gun, operating with 300 W (12 kV/25 mA) power. The spectra were collected in the region of the Pt4f, Ru3p, Cl2p and O1s levels. The binding energies were then corrected for the surface-charging effects during the measurements by using the C1s core level (284.6 eV) of the adventitious carbon as an internal reference. A flood gun with electron acceleration at 1 eV and electron current of 100 μA was used in order to avoid charge effects. Photoelectrons were recorded in normal emission by using a Phoibos 150 analyzer, operating with a pass energy of 30 eV. The XPS spectra were fitted by using Voigt profiles combined with their primitive functions, for inelastic backgrounds. The Gaussian width of all lines and thresholds was the same for one spectrum and do not differ considerably from one spectrum to another, being always in the range of 2 eV.

Electron microscopy (TEM-HRTEM) experiments were carried out in a JEOL 2011 high resolution transmission electron microscope operating at 200 kV, with a point resolution of 0.23 nm and C_s = 1.0 mm. The instrument was also equipped with an Oxford Instruments INCAx-sight liquid nitrogen-cooled energy dispersive X-ray spectroscopy (EDS) detector with an Si(Li) window for chemical analysis of the samples. Qualitative and semi-quantitative analysis of EDS data was accomplished using the INCA Microanalysis Suite software. Samples were prepared by gently grinding the catalyst in high-purity ethanol using an agate pestle and mortar. A drop of the suspension was subsequently deposited onto a lacey carbon-film supported on a Cu grid and allowed to evaporate under ambient conditions.

Boehm titration was used to determine the total number of acid sites of carbon catalysts in aqueous solution. Suspensions of the catalyst samples in aqueous 0.01 N NaOH solutions (0.25 g in 25 mL solution) were agitated for 24 h at room temperature in a shaker bath for neutralization of the acidic sites by the base. The solids were then separated with vacuum filtration and 10 mL of the filtrate was titrated with aqueous HCl solution (0.01 N). During titration the pH change of the base solution was continuously monitored with a pH meter. The qualitative determination of the neutralization point was determined by a sharp color change of the solution, using an appropriate indicator (methyl red) in combination with a sharp change in pH. For the quantitative determination of the catalyst's acid sites, the method of second derivative was applied to calculate the equilibrium point. Blank titration experiments, i.e. without the use of the solid acid catalysts, were also conducted with the respective 0.01N HCl and NaOH solutions [63,64].

2.3. Catalytic tests

2.3.1. Hydrolytic hydrogenation of cellulose

A commercial microcrystalline cellulose (Avicel PH-101, Fluka) with particle size ~50 μm was used as received in all the hydrolytic hydrogenation experiments of the current study. The catalytic tests were carried out in batch mode according to the following procedure: 0.48 g of catalyst, 1.12 g cellulose and 40 mL of deionized water were loaded in a high-pressure autoclave reactor (100 mL, Parr, Monel 400), flushed three times with pure hydrogen and heated to 180 °C under relatively low H_2 pressure (2.0 MPa, at room temperature) and vigorous stirring (600 rpm). The experiments took place at these conditions for 24 h. In addition, the effect of hydrogen pressure was tested by performing experiments at initial (room temperature) pressures of 2, 6 and 9 MPa, at constant temperature of 180 °C.

The effect of cellulose crystallinity and morphology was also studied, by using a ball-milled sample of Avicel as feed. The milling of initial micro-crystalline cellulose was performed with a 200 mL stainless steel (SS) cylindrical container using SS balls at rotating speed of 100 rpm for 44 h.

After reaction, the solids (mixture of catalyst with unreacted cellulose) were filtered off and the filtrate solution was analyzed by

high pressure liquid chromatography (HPLC, Shimadzu) by using refractive index (RI) detector (RID-6A) and a SH-1011 Sugar Column (Shodex) with solution of 0.01N H_2SO_4 in ultrapure H_2O (0.7 mL/min, 45 °C) as the mobile phase. The quantification was based on external calibration standard solutions of sugar alcohols, sugars, furans, organic acids and aliphatic alcohols. As some isomers cannot be separated by this HPLC column, the sum of sorbitol and mannitol is reported as total C6 sugar alcohols (hexitols), the sum of arabinitol and xylitol as total C5 sugar alcohols (pentitols), and the sum of threitol and erythritol as total C4 sugar alcohols. However, in order to obtain information regarding the ratio of these isomers, representative measurements were also performed by ion chromatography (ICS-5000, Dionex, USA) using a CarboPac PA1 (5 mm, 4 × 250 mm) column and precolumn (5 mm, 4 × 30 mm) connected to a pulsed amperometric detector (PAD); the filtrate solutions were analyzed without further treatment.

The conversion of cellulose was determined based on the weight difference of dried cellulose before and after the reaction (after subtracting the catalyst weight used each time):

$$\text{Cellulose conversion}(\%) = \left[1 - \frac{m_{\text{unreacted cellulose}}}{m_{\text{cellulose feed}}}\right] \times 100$$

The conversion of cellulose based on total organic carbon (TOC, Shimadzu TOC-VCSH analyzer; detection limit 0.1 mg/L and relative standard deviation ≤ 5%) measurements of the liquid products was also determined for representative catalytic runs and the obtained values were compared to those from the weight difference method, in order to identify any possible formation of humins.

The selectivity to the various products was determined on the basis of carbon moles of each product (measured by HPLC analysis) and the moles of total carbon converted (determined as glucose units), using the equation below, i.e. for the case of sorbitol:

$$S_{sorbitol}(\%) = (mol\,C\ of\ sorbitol/mol\ of\ total\ C\ converted) \times 100$$

In order to determine the moles of total C converted, the C moles of initial and non-converted cellulose were estimated by the equation:

$$C\ moles\ of\ cellulose = [mass\ of\ cellulose/(0.9 \times 180.16)] * 6$$

The yield of products was estimated from their mass and the mass of initial cellulose used, with the following equation:

$$Yield(\%) = (m_{product}/m_{\text{cellulose feed}}) \times 100$$

The bifunctional catalysts (5% Ru/AC-SO_3H & 5% Pt/AC-SO_3H) were also evaluated for their stability and reusability in the hydrolytic hydrogenation of microcrystalline cellulose at 2 MPa hydrogen pressure, for 24 h at 180 °C. After the 1st run, the catalyst and the unreacted cellulose were recovered by filtration, and then fresh cellulose was added to the solid mixture to compensate for the converted cellulose. The resulting mixture was subjected to reaction under the same conditions. This procedure was repeated up to four runs.

2.3.2. Hydrogenation of D-glucose

The D-glucose (Riedel-de Haën) hydrogenation experiments were performed at 180 °C for 3–24 h at relatively low H_2 pressure (2.0 MPa) in the same high-pressure autoclave reactor (Parr, 100 mL) under vigorous stirring (600 rpm). In a typical run, 1.12 g of D-glucose, 0.48 g of catalyst and water (40 mL) were charged in the reactor. After reaction, the mixture was cooled and the catalyst was separated by vacuum filtration. The liquid products were analyzed by HPLC with the same methods as described above. The conversion of D-glucose was determined based on the initial and final moles of glucose (determined by HPLC) before and after reaction, using the following equation:

$$\text{Glucose conversion}(\%) = \left[1 - \frac{\text{moles}_{\text{unreacted glucose}}}{\text{moles}_{\text{charged glucose}}}\right] \times 100$$

The selectivity to the various products was determined as for the cellulose experiments above.

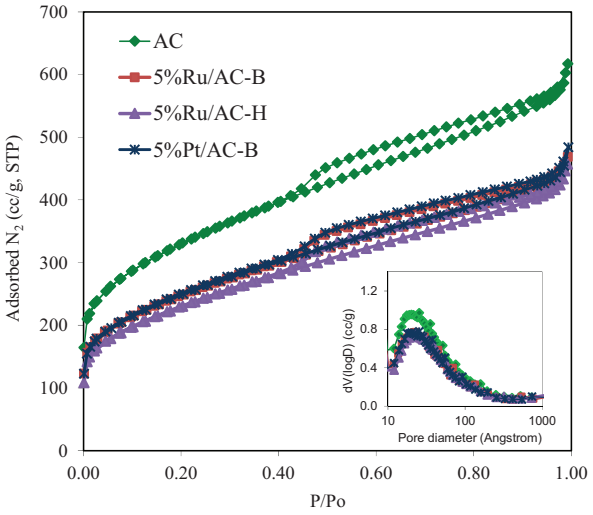

Fig. 1. N_2 adsorption-desorption isotherms and pore size distribution curves (BJH, adsorption data) of the parent activated carbon (AC) and representative supported Ru and Pt catalyst samples.

3. Results and discussion

3.1. Physicochemical characteristics of the catalysts

The metal content of the prepared Ru or Pt/AC catalysts, reduced either with $NaBH_4$ or with H_2, the specific surface area (BET) and micropore area (t-plot), and the total acidity (Boehm titration) are shown in Table 1. The successful grafting of sulfonic groups (–SO_3H) on the catalysts treated with c. H_2SO_4 was verified by means of S elemental analysis (Table SI-1 in the Supporting information). The activated carbon (AC) used as catalyst support is a micro/mesoporous carbon with high contribution of mesoporosity. As can be seen in Table 1, only ~28% of its total surface area corresponds to micropore area, the rest being mainly mesopore as well as macropore and external surface area. This can be also revealed from the shape of the N_2 isotherms shown in Fig. 1, where a progressive increase of adsorbed N_2 can be observed over the whole P/Po range, thus indicating the presence of relatively disordered network of meso- and macropores. The pore size distribution based on BJH analysis (shown as inset in Fig. 1) and DFT analysis (not shown for brevity) of the adsorption data show the presence of mesopores with sizes up to ca. 10 nm with average size at ~3 nm. Considering that the kinetic diameter of glucose is ~0.8 nm (8 Å), with the various intermediate and final targeted products (i.e. sorbitol, smaller sugar alcohols and glycols) having similar or smaller sizes, it is expected that such an activated carbon with abundant mesopores would exhibit improved transport properties, thus minimizing secondary hydrogenolysis, dehydration or epimerization reactions and increasing conversion rates and desorption of primary products (i.e. sorbitol). The surface area of the metal loaded AC catalysts has been reduced by ca. 30% max compared to that of the parent activated carbon (Table 1), thus indicating that the texture and porosity of the carbon support has not been significantly altered throughout the catalyst preparation steps. This is also revealed by the identical shapes of the N_2 isotherms and pore size

Table 1
Physicochemical properties of the Pt or Ru/AC catalysts.

Catalyst	Metal content (wt.%)[a]	Total acidity (mmoles/g)[b]	Specific surface are (m^2/g)[c]	Total pore volume (P/Po = 0.99) (cm^3/g) [d]
AC	–	0.220	1182 (335)	0.954
AC-SO_3H	–	0.665	965(230)	0.796
1%Ru/AC-B	0.78	0.380	906 (294)	0.730
3%Ru/AC-B	2.45	0.445	1057 (337)	0.826
5%Ru/AC-B	4.84	0.575	882 (243)	0.725
1%Ru/AC-H	0.87	0.500	715 (137)	0.638
3%Ru/AC-H	2.78	0.715	835 (183)	0.721
5%Ru/AC-H	4.82	0.975	822 (183)	0.707
1%Ru/AC-SO_3H	0.72	0.625	1108 (207)	0.890
3%Ru/AC-SO_3H	2.15	0.665	950 (205)	0.780
5%Ru/AC-SO_3H	4.35	0.690	882 (199)	0.711
1%Pt/AC-B	0.96	0.992	965 (281)	0.777
3%Pt/AC-B	2.41	1.200	872 (172)	0.706
5%Pt/AC-B	4.75	1.022	889 (238)	0.748
1%Pt/AC-H	0.85	0.926	945 (287)	0.832
3%Pt/AC-H	2.85	0.618	905 (214)	0.774
5%Pt/AC-H	4.80	0.729	914 (201)	0.758
1%Pt/AC-SO_3H	0.92	0.910	946 (209)	0.760
3%Pt/AC-SO_3H	2.36	0.900	994 (254)	0.789
5%Pt/AC-SO_3H	4.68	1.120	743 (202)	0.583

[a] Determined by ICP-AES.
[b] Measured by Boehm titration.
[c] Total surface area determined by N_2 sorption at 77 K and multi-point BET analysis in P/Po range of 0.05–0.25. The numbers in parentheses refer to the micropore area (by t-plot analysis), the rest being meso/macropore and external surface area.
[d] Total pore volume determined by N_2 sorbed at P/Po = 0.99.

distribution curves of the parent AC and representative catalysts with the highest metal loading, i.e. 5% Pt or Ru, shown in Fig. 1.

With regard to acidity as determined by Boehm titration, it can be seen from the data in Table 1 that the total acidity of the parent AC increased substantially after sulfonation, as it was expected. This was also roughly verified by simple pH measurements of AC-water suspensions, which showed the values of ~9.5 for the parent AC and ~2.8 for AC-SO_3H. Incorporation of metals (both Pt and Ru) and subsequent treatment/reduction either with $NaBH_4$ or in H_2 at 350 °C resulted also in increased acidity compared to that of the parent AC, as was also previously reported [38]. In addition to the effect of the Ru and Pt metals and their oxides (their presence was verified by the XPS and TEM results), the contribution of remaining chlorine ions on the catalyst surface (see also discussion below) could be another reason for the increased acidity of the catalysts. The pH of the water suspensions of the Ru or Pt catalysts supported on the parent AC was in the range of 5.5–6.0, compared to 9.5 of the neat AC. Accordingly, the pH values of the Pt or Ru/AC-SO_3H water suspensions were in the range of 3.5–5.0. The higher pH values of the metal/sulfonated catalysts compared to that of the parent AC-SO_3H (2.8) is attributed to the treatment of the catalysts with $NaBH_4$ which was performed in order to reduce the supported Ru and Pt metals.

The XRD patterns of the Ru and Pt/AC catalysts reduced by $NaBH_4$ or H_2 at 350 °C are shown in Fig. 2. No characteristic diffraction peaks of metallic (or oxide) species can be observed in the XRD patterns for the 1% and 3 wt.% metal loaded catalysts, for both Ru and Pt, irrespective of the reduction method applied. The absence of the diffraction peaks indicates either the presence of metal or metal oxide crystallites smaller than ca. 3 nm or the absence of any crystalline phase. In the case of the 5% Pt catalysts, the Pt(111) reflection can be clearly observed in the patterns of both the $NaBH_4$ and H_2 reduced catalysts, thus indicating an increase of the crystal size. The Ru(101) and RuO_2(101) reflections can be hardly identified only in the 5% Ru catalyst reduced by $NaBH_4$. These results have been also verified by the HRTEM analysis of the catalysts as shown below.

In order to further investigate the metal particle size distribution and its crystalline nature, the catalysts were characterized by TEM and HRTEM measurements. A representative TEM image of the 1% Ru/AC-B catalyst (reduced by $NaBH_4$) is shown in Fig. 3(a). The Ru nanoparticles, depicted in the image with black and white arrows, are evenly dispersed on the AC support. The majority of the nanoparticles are ≤2–3 nm (black arrows) while a few aggregates (dark grey areas) with size of up to ca. 25 nm were also observed (white arrows). These dark grey areas predominately comprised of metallic Ru surrounded by –and agglomerated with- oxygen enriched ruthenium amorphous phases, i.e. $Ru(O)_x^{\delta+}$, based on selected area diffraction (SAD) and energy dispersive spectroscopy (EDS) measurements, as was also described in our previous work [52]. The presence of tiny Ru nanoparticles was confirmed by EDS chemical analysis at different areas of the sample and at varying magnifications. The oxidation state of Ru was verified by selected area diffraction (SAD) patterns, such as the one shown as inset in Fig. 3(a) for an aggregated Ru area. Measurement of the diffraction spots spacing resulted in d = 0.306 nm, which is attributed to the (001) crystal planes of RuO_2. Metallic Ru nanoparticles were also identified by HRTEM observations but represented a rather smaller fraction of the catalyst. Microscopy observations performed for the 3 and 5% Ru/AC-B catalysts revealed analogous results (data not shown for brevity). In addition, similar morphology and sizes were also observed for the respective Ru/AC-H catalysts that have been reduced with H_2 at 350 °C (instead of using $NaBH_4$). The TEM image of the 5% Ru/AC-H catalyst is shown in Fig. 3(b). Tiny Ru nanoparticles of ≤2–3 nm (pointed by black arrows) and larger agglomerated ones of ca. 15–20 nm (white arrows) were identified. Ruthenium predominately exists in metallic form, contrary to the respective $NaBH_4$ reduced samples, as deduced by the SAD pattern inset in Fig. 3(b), where the $10\bar{1}1$ reflection of the hexagonal Ru is shown, having an interplanar spacing of $d_{10\,\bar{1}1}$ = 0.2055 nm. RuO_2 phases were also identified but to a lower proportion.

The Pt nanoparticles on the 1%Pt/AC-B catalyst (reduced by $NaBH_4$) exhibited a uniform almost spherical morphology with relatively narrow size distribution of about 2–3 nm and even dispersion on the carbon surface, as can be seen in Fig. 3(c). The lattice fringes of the particles in the inset of Fig. 3(c) have an average experimental spacing of 0.225 nm, which matches quite well with that of the {111} planes of Pt. Therefore, the formation of metallic Pt species is undoubtedly verified. In comparison to the Ru particles on the respective catalyst samples, the Pt particles appeared to be more crystalline, as identified by the clearly resolved lattice fringes

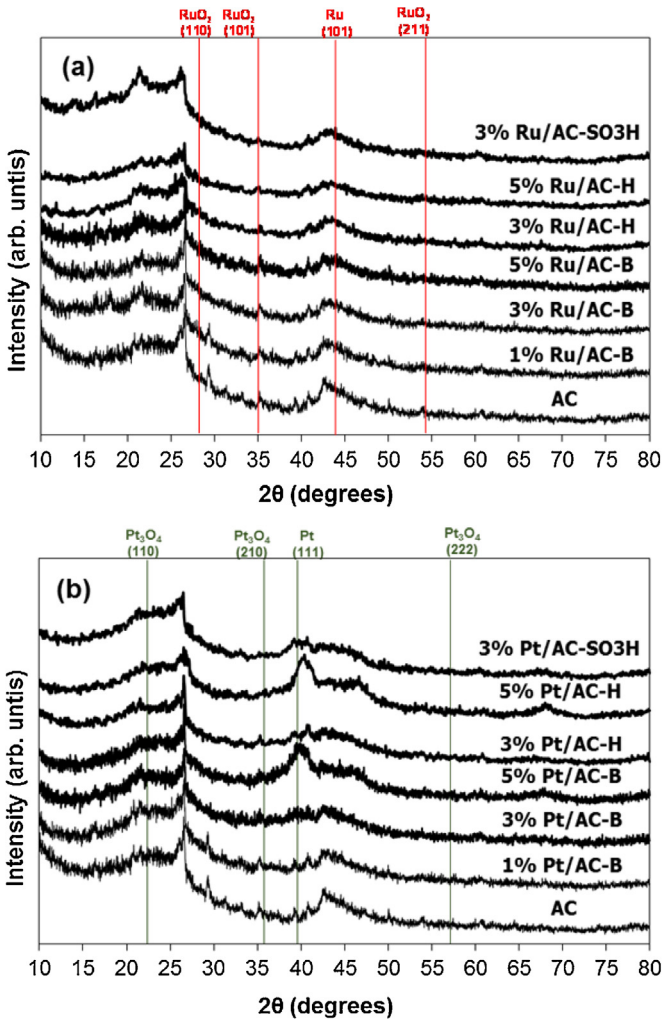

Fig. 2. XRD patterns of the parent activated carbon (AC) and representative catalysts: (a) Ru/AC-B and Ru/AC-SO_3H which were reduced with $NaBH_4$ and Ru/AC-H which were reduced with H_2 at 350 °C, and (b) the corresponding Pt/AC-B and Pt/AC-SO_3H catalysts. The 2θ locations of the most intense reflections of the reference XRD patterns for metallic Ru(hexagonal), RuO_2(tetragonal), Pt (cubic) and Pt_3O_4(cubic) are also denoted with red (Ru) or green lines (Pt), respectively, in order to verify the absence/presence of such crystalline phases. (For interpretation of the references to colour in this figure legend, the reader is referred to the web version of this article.)

in the images of the latter particles. However, at higher loadings, especially at the 5%Pt/AC-B catalyst, in addition to the small Pt particles of ca. ≤4 nm, several aggregates of up to ca. 25–30 nm were observed, as can be seen in Fig. 3(d). Furthermore, dark grey aggregates of small crystalline Pt particles surrounded by amorphous oxygen-rich areas, were also identified (inset of Fig. 3(d)), similar to the Ru/AC catalysts. In the Pt/AC-H catalysts, reduced by H_2 at 350 °C, a uniform distribution of small crystalline metallic Pt particles (with narrow size distribution and average size of 2–3 nm) was also observed, with lower degree of aggregation at higher loadings, compared to the $NaBH_4$ reduced catalysts.

X-ray photoelectron spectroscopy (XPS) measurements (Fig. 4, Table SI-2 in the Supporting information) showed the existence of both metallic and oxidic surface species, in different proportions, depending on the reduction method (i.e., $NaBH_4$ or H_2 at 350 °C) and the amount and type of metal. Reduction with hydrogen led to incomplete removal of chlorine and partial reduction of both metals, i.e. Ru and Pt. Indeed, as can be seen in Fig. 4, the XPS spectra of the Ru/AC-H catalysts for the Ru3d level showed the presence of Ru species both in metallic and oxidized states, as evidenced by the metallic Ru (280.5 eV) and Ru-O (281.6 eV) bands after deconvolution of the spectra. The observation of the Ru-Cl band (282.1 eV) revealed also the presence of ruthenium salt ($RuCl_3$) remnants. Analysis of the Ru3p region (spectra not shown) verified the presence of metallic Ru (band at 459.8 eV), Ru-O (band at 462.2 eV) and Ru-Cl (band at 463.2 eV). Reduction of the catalysts with $NaBH_4$ led to relatively lower presence of chlorine ions, while the metal was again not effectively reduced to $M^{(0)}$, as can be seen in the respective spectra of the Ru/AC-B samples in Fig. 4. The presence of chlorine ions on the catalysts was also verified by TPD-MS experiments (not shown) in which the masses of Cl_2 and HCl were detected in the gas products. The oxidation state ratio data (i.e. $Ru^{(0)}$/RuOx), derived from the peak deconvolution of the respective XPS spectra, are presented in Table SI-2 in the Supporting information. Metallic $Ru^{(0)}$ was negligible on the surface of the $NaBH_4$ reduced catalysts, while in the H_2 reduced catalysts, the percentage of $Ru^{(0)}$ species didn't exceed ca. 30%, the highest being measured for the low Ru loading (1%Ru/AC-H). Similar results were derived from the XPS analysis of the Pt/AC catalysts (the respective data are also shown in Table SI-2 in the Supporting information). The maximum value of $Pt^{(0)}$ was 21% and was observed for the lower Pt loading, i.e. the 1%Pt/AC-H which was reduced with H_2. This difference in Ru and Pt reducibility between the $NaBH_4$ and H_2 treated catalysts is in accordance with the HRTEM results discussed above, where more well-formed crystalline nanoparticles were generally observed in the H_2 reduced catalysts.

3.2. Hydrolytic hydrogenation of microcrystalline cellulose

The successful selective transformation of cellulose to sugar alcohols requires the development of catalytic materials with the ability to induce fast hydrolysis of cellulose to glucose followed by its hydrogenation to hexitols which may then be converted via hydrogenolysis to smaller sugar alcohols. A retro-aldol reaction step leading to C2–C4 intermediates directly from glucose followed by their hydrogenation to the respective alcohols has been also proposed. The balance between initial cellulose hydrolysis, retro-aldol and hydrogenation/hydrogenolysis reaction rates is crucial and is governed by the nature of the catalyst active sites (acid sites and metal hydrogenation sites) and reaction conditions (cellulose to catalyst ratio, initial cellulose concentration, pretreatment of cellulose to reduce crystallinity, temperature, time, hydrogen pressure, acidity of reaction media). In addition, to the above reaction pathways, a bifunctional catalyst with relatively acidic support or the simultaneous use of two catalysts, one with acidic function and one with hydrogenation activity, would also enhance the dehydration of formed sorbitol towards other products such as sorbitan and isosorbide [4,20,22,30,65–70]. A generalized scheme of the various reaction steps in the hydrolytic hydrogenation of cellulose is shown in Fig. 5.

The results of the hydrolytic hydrogenation of microcrystalline cellulose with the Ru and Pt/AC, as well as the bifunctional Ru & Pt/AC-SO_3H catalysts, at 180 °C under relatively low hydrogen pressure (2.0 MPa measured at room temperature) are shown in Table 2 and Table SI-3 (Supporting information). In the absence of any solid catalyst, an appreciable conversion of cellulose occurred (~24.8%), leading to the formation of glucose and arabinose as well as various degradation products, such as HMF, levulinic acid, lactic acid, formic acid, etc. As discussed in the introduction, the hot compressed water conditions induce the formation of acidic hydronium ions (H_3O^+) which can initiate cellulose hydrolysis and further glucose conversion reactions. However, it is clear from the data in Table 2 that the carbon balance in the non-catalytic experiment is not very high (~65%), when only the HPLC analysis data are considered. Furthermore, when the conversion was estimated on the basis of the HPLC determined monomeric compounds, it was 9.6%, thus indicating the existence of soluble oligomers in the samples (Table

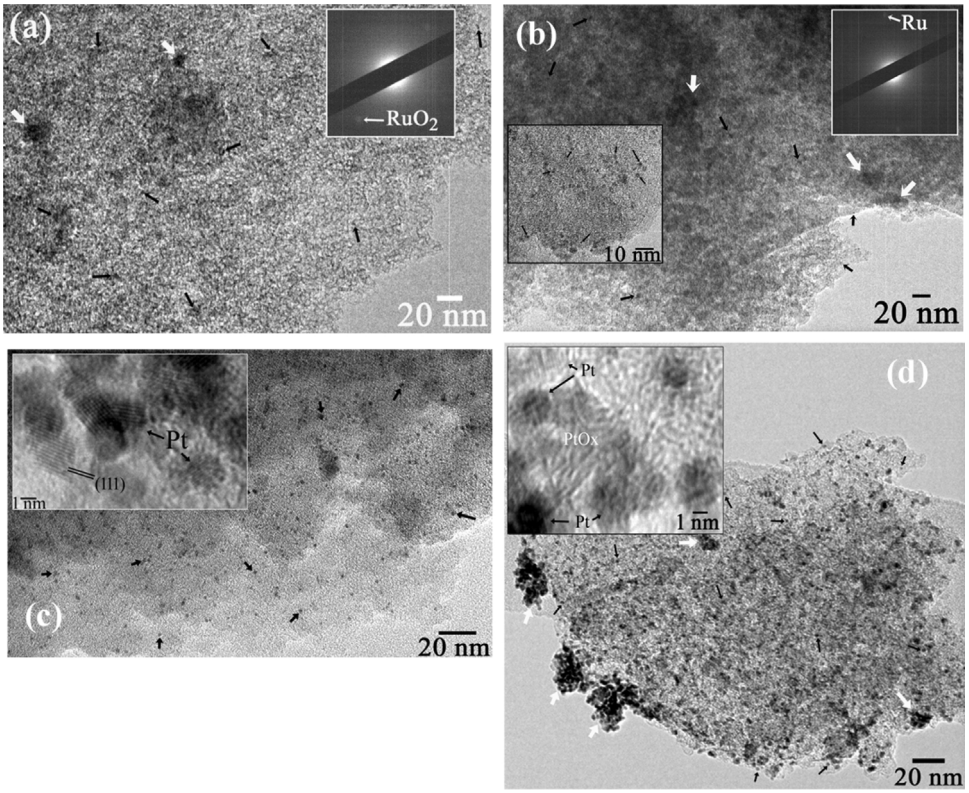

Fig. 3. TEM images of the Ru catalysts: (a) 1% Ru/AC-B, (b) 5% Ru/AC-H, (c) 1%Pt/AC-B, and (d) 5%Pt/AC-B along with their corresponding SAD patterns (in a, b) and high-resolution images (in b–d) presented as insets. The differences in the size range of Ru or Pt particles are denoted by white (larger particles) and black (tiny ones) arrows, respectively.

Table 2
Catalytic results of microcrystalline cellulose hydrolytic hydrogenation with Ru and Pt/AC catalysts reduced with $NaBH_4$ (B series) or H_2 at 350 °C (H series) and with bifunctional catalysts (Ru & Pt/AC-SO_3H).

Catalyst	Cellulose conversion (wt.%)	Selectivity (carbon based, % on total converted carbon)							
		C_5–C_6 sugars & cellobiose	Sugar degradation products[a]	Sugar alcohols[b]					
				EG	Gly	C_3 diols	C_4	C_5	C_6	Total sugar alcohols
–	24.8	37.0	28.5	–	–	–	–	–	–	
AC	26.2	15.4	13.2	–	–	–	–	–	–	
AC-SO_3H	34.4	22.0	43.4	–	–	–	–	–	–	
1%Ru/AC-B	30.9	4.7	4.9	3.4	15.5	8.2	3.1	5.0	2.2	37.4
3%Ru/AC-B	29.2	2.2	3.7	1.6	4.5	5.6	2.3	3.0	2.8	19.8
3%Ru/AC-H	27.0	3.9	2.6	0.3	5.4	1.1	3.3	4.6	4.4	19.1
5%Ru/AC-B	36.7	3.9	7.7	11.6	9.6	2.9	–	6.6	24.6	55.3
1%Ru/AC-SO_3H	28.8	3.0	3.2	0.9	1.8	5.2	–	1.6	3.3	12.8
3%Ru/AC-SO_3H	31.9	3.5	–	0.1	4.3	–	3.9	10.0	33.9	52.2
5%Ru/AC-SO_3H	38.3	2.0	0.8	0.3	2.8	0.9	–	5.0	31.7	40.7
1%Pt/AC-B	36.2	5.5	6.9	1.8	14.4	5.4	–	4.8	5.1	31.5
3%Pt/AC-B	27.9	5.2	5.4	0.4	6.6	1.1	–	4.5	13.9	26.5
3%Pt/AC-H	26.6	6.1	0.6	1.1	6.5	2.2	1.8	7.9	10.8	30.3
5%Pt/AC-B	24.1	5.9	2.0	0.7	6.7	1.8	–	5.8	14.3	29.3
1%Pt/AC-SO_3H	29.5	5.0	3.4	0.9	5.6	1.2	–	3.5	17.3	28.5
3%Pt/AC-SO_3H	32.0	2.6	1.9	0.4	3.1	0.2	–	5.7	34.5	43.9
5%Pt/AC-SO_3H	46.9	1.8	3.2	–	2.0	–	–	5.1	40.2	47.3

Reaction conditions: 0.48 g cat., 1.12 g microcrystalline cellulose, 2 MPa H_2, 40 mL water, 180 °C, 24 h (2% standard deviation for selectivity values).

[a] Sugar degradation products: HMF, formic acid, levulinic acid, lactic acid, succinic acid, acetic acid, propionic acid, R-OH (aliphatic alcohols, i.e. MeOH, EtOH).

[b] C4 sugar alcohols: sum of threitol and erythritol; C5 sugar alcohols: sum of arabinitol and xylitol; C6 sugar alcohols: sum of sorbitol and mannitol; EG: ethylene glycol; Gly: glycerol; C3 diols: propane-1,2-diol (propylene glycol) and propane-1,3-diol.

SI-4, Supporting information). The TOC data (Table SI-4) which take into account both the monomeric biomass derived compounds as well as any soluble oligo-saccharides, showed higher conversion (~17%) compared to that based on HPLC but still lower compared to that determined by the weight difference method (24.8%). All the above, together with the observed dark brown colour of cellulose, indicate also the extensive formation of carbonaceous humins in the non-catalytic hydrolysis experiments, in accordance with previous related reports [71,72]. The transformation of the glucose units to more condensed carbon structures was also verified by the elemental analysis of cellulose prior and after the non-catalytic hydrolysis experiments, i.e. 42.1 wt.% C and 6.1 wt.% H for the parent cellulose and 64.5 wt.% C and 4.8 wt.% H for the remaining cellulose after hydrolysis. When the neat activated carbon (AC) was added,

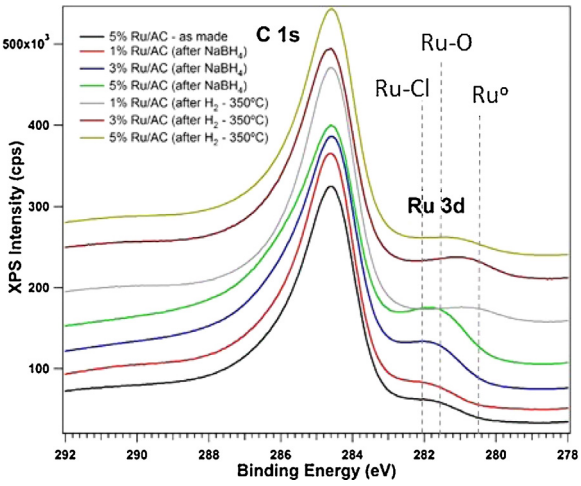

Fig. 4. XPS spectra of Ru3d for the Ru/AC catalysts reduced with $NaBH_4$ or H_2 at 350 °C.

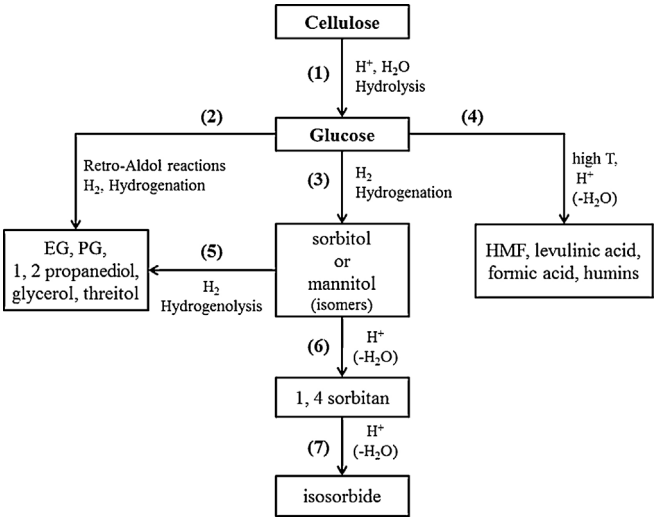

Fig. 5. Generalized scheme of reaction steps in hydrolytic hydrogenation of cellulose with bifunctional (metal/acid) catalysts.

the increased basicity of its surface (pH in water 9.5 at 25 °C) had no significant effect on cellulose conversion (26.2%) but induced different product selectivity compared to the non-catalytic experiment, favoring mostly the formation of organic acids instead of HMF, as well as of aliphatic alcohols such as ethanol (Tables 2 and SI-3). The conversion based on HPLC analysis was only 6.5% (with 29% carbon balance) and 13% based on the TOC data (Table SI-4), indicating again the formation of soluble oligomers and carbonaceous humins. As expected, the use of the acidic sulfonated carbon (AC-SO_3H) offered an increased cellulose conversion of 34.4% with glucose, arabinose, HMF, formic and lactic acids being the main products (Tables 2 and SI-3). The conversion based on HPLC analysis was 22% (with 65% carbon balance) and 25% based on the TOC data (Table SI-4). The gas products contained very small amounts of CO_2 (<1%v/v) and C1-C4 hydrocarbons (<0.1%v/v), the rest being the reactant H_2.

Interestingly, the metal (Ru or Pt) –loaded catalysts of the parent AC (non sulfonated carbon) exhibited increased cellulose conversion compared to the AC alone (Table 2). This can be attributed to the increased acidity of the metal-loaded AC catalysts, as measured by Boehm titration (Table 1). With regard to Ru/AC catalysts, the conversion ranged from 27% to 36.7%, being higher at higher (5 wt.%) Ru loading, while the H_2 reduced catalysts appeared to be

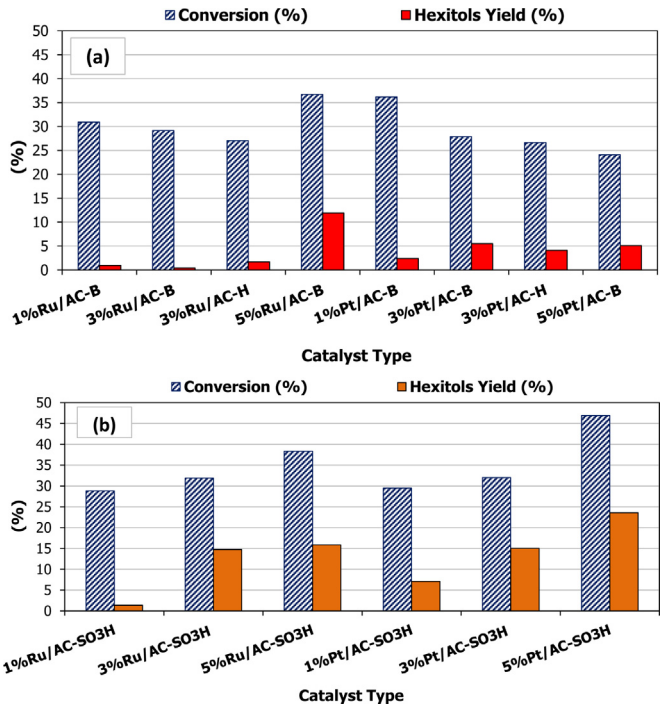

Fig. 6. Microcrystalline cellulose conversion (wt.%) and hexitols yield (wt.%) for the various Ru & Pt/AC catalysts supported on (a) the parent, non-sulfonated carbon (AC) and reduced with $NaBH_4$ (B) or H_2 (H) at 350 °C, and (b) the sulfonated carbon (AC-SO_3H) and reduced with $NaBH_4$ (reaction conditions: 0.48 g cat., 1.12 g cellulose, 2 MPa H_2, 40 mL water, 180 °C, 24 h).

slightly less reactive compared to the $NaBH_4$ reduced ones (Table 2). As expected, the composition of the liquid products was dominated by sugar alcohols, such as hexitols (sorbitol and mannitol), pentitols (arabinitol and xylitol), C4 sugar alcohols (threitol and erythritol), C3 diols (mainly propane-1,2-diol), glycerol and ethylene glycol. Aliphatic alcohols, such as methanol and ethanol, were also produced. Total sugar alcohol selectivity ranged between 19.1 and 55.3%, with total carbon balance being between 26% and 67%. As a general trend, the higher Ru loading favoured the formation of hexitols (selectivity ranged from 2.2 to 24.6%). On the other hand, the selectivity to smaller sugar alcohols was relatively high with the 1 wt.%Ru/AC-B catalyst (glycerol selectivity reached 15.5%), it was generally reduced with the 3 wt.% Ru catalysts, and was increased again at 5 wt.%Ru. This is indicative of the different reaction mechanisms that prevail depending on the metal content and the balance between the acid and hydrogenation function of the catalysts, as discussed further below. Comparing the Ru reduction methods, the H_2 reduced catalysts seemed to slightly favour the formation of C4-C6 sugar alcohols compared to those reduced with $NaBH_4$.

The Pt/AC catalysts afforded similar cellulose conversion (from 24.1% to 36.2%), with the total selectivity to sugar alcohols ranging between 26.5% and 31.5% (total carbon balance 37%–43.9%). The C6 sugar alcohols selectivity ranged from 5.1 to 14.3% and was higher at high Pt loadings (i.e. 3 and 5 wt.%), while the smaller alcohols showed high selectivity with the 1 wt.%Pt/AC-B catalyst (i.e. selectivity for glycerol was 14.4%) which was decreased with the 3 and 5 wt.%Pt catalysts. The data of cellulose conversion and hexitols (sorbitol and mannitol) yield, for all the catalysts supported on the parent AC, are shown in Fig. 6(a). Although conversion reached appreciable levels (i.e. up to 37%) considering the recalcitrance nature of microcrystalline cellulose (Avicel), the yield of hexitols remained below ca. 12 wt.%.

The catalytic results of the metal-loaded sulfonated (Ru or Pt/AC-SO_3H) catalysts are also shown in Table 2 (and Table SI-3

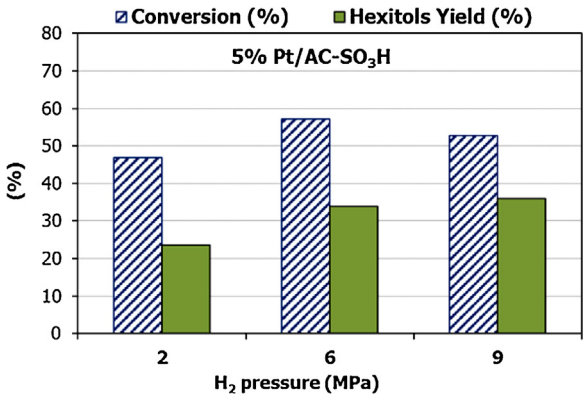

Fig. 7. Effect of H_2 initial pressure on microcrystalline cellulose conversion (wt.%) and hexitols yield (wt.%) using 5% Pt/AC-SO_3H bifunctional catalyst.

in the Supporting information). In the case of the Ru/AC-SO_3H catalysts, the conversion of microcrystalline cellulose ranged between 28.8% and 38.3% and was similar to that obtained with the metal-loaded non-sulfonated AC catalysts, despite the higher acidity of the Ru/AC-SO_3H catalysts. On the other hand, the selectivity towards sugar alcohols was different between these two sets of catalysts, with the AC-SO_3H supported catalysts producing significantly more hexitols (selectivity ranged from 3.3 to 33.9%) and less glycerol compared to the non-sulfonated Ru/AC catalysts. Similar effects where observed with the Pt/AC-SO_3H catalysts compared to the corresponding non-sulfonated Pt/AC catalysts. They exhibited higher C6 sugar alcohols selectivity (ranged from 17.3 to 40.2%) and lower selectivity to smaller alcohols, with the 5%Pt/AC-SO_3H catalyst being the most active (46.9% cellulose conversion) and selective towards hexitols (40.2%). The data of cellulose conversion and hexitols yield, for all the catalysts supported on sulfonated carbon, are shown in Fig. 6(b). The production of C_6 sugar alcohols (1.3–23.6% yield) was higher compared to that with the corresponding non-sulfonated catalysts, with the 5%Pt catalyst being more efficient compared to the 5%Ru catalyst (i.e. 23.6% vs. 15.8% hexitols yield). The increased hexitols yield with the sulfonated catalysts was mainly attributed to the increased selectivity towards hexitols since cellulose conversion was more or less similar to that obtained with the non-sulfonated catalysts (Fig. 6a and b).

The carbon balance with all the Pt or Ru catalysts supported on the parent AC or on AC-SO_3H, ranged from 19% to 67% (Table 2), while the conversion estimated on the basis of HPLC data (monomers) was about 50% less (in average) compared to that found by the weight difference method. Thus, the presence of soluble oligo-saccharides as well as the formation of carbonaceous humins can be also suggested here as in the case of the hydrolysis experiments described above. However, in the case of the hydrolytic hydrogenation experiments, an additional factor that leads to decreased carbon balance when only the liquid products are considered, is the substantial formation of gaseous products. For example, the gas products in the experiment with 5%Ru/AC-SO_3H contained 50.3%/v/v methane, 6.6%v/v C2-C4 hydrocarbons, 8.2%v/v CO_2, the rest being the reactant H_2.

3.3. Effect of hydrogen pressure

The effect of hydrogen pressure in the hydrolytic hydrogenation of microcrystalline cellulose was studied by the use of 5%Pt/AC-SO_3H bifunctional catalyst which, as shown above, was the most effective catalyst for C_6 sugar alcohols production. The obtained results regarding cellulose conversion and sorbitol yield are shown in Fig. 7. A moderate increase of cellulose conversion from 47 to 57% was observed by increasing the pressure from 2 to 6 MPa, while further increase to 9 MPa had no additional positive effect. The same trend was observed for the yield of hexitols, which was enhanced from 23.6% at 2 MPa to 33.9% at 6 MPa and 35.9% at 9 MPa. Such a favorable performance towards sorbitol production at low H_2 pressure was also previously reported for the 3wt%Ru/BEA and 3wt%Ir-BEA zeolite based catalysts [45]. Also, a 2 wt.%Ru/AC catalyst was quite effective in the hydrolytic hydrogenation of ball-milled cellulose towards the production of sorbitol at 0.8 MPa H_2 pressure [36]. High yield of sorbitol (ca. 54%) from pretreated cellulose was also obtained at H_2 pressure of 0.7 MPa and 60 °C but in this case the catalyst comprised of Pt nanoparticles (24% mole to cellulose) in acidic medium of 0.7 M aq. $H_4SiW_{12}O_{40}$ [73].

3.4. Effect of cellulose pretreatment (ball-milling)

The recalcitrant nature of cellulose is attributed to its relative high crystallinity compared to other polysaccharides such as hemicellulose, starch, etc. A common mechanical-physical method to reduce cellulose's crystallinity and facilitate its dissolution and hydrolysis to glucose monomers is ball milling. The XRD patterns of Fig. 8(a) show how microcrystalline cellulose (Avicel) can become amorphous after milling for 44 h with stainless steel mill and balls. This pretreatment affects also the morphology and size of cellulose microparticles as can be seen in the SEM images of Fig. 8(b) and (c). The parent microcrystalline cellulose comprised of needle-type primary particles aggregated to larger secondary particles with lengths of >50 μm. After ball-milling, "broken" particles with more spherical shapes and sizes of less than ca. 30 μm were formed.

The effect of cellulose ball milling and its amorphization on its hydrolysis and hydrolytic hydrogenation with the various metal or bifunctional catalysts is shown in Tables 3 and SI-5 (Supporting information), as well as in Fig. 9. Even in neat water, under the hydrothermal conditions applied in this work, conversion increased from 24.8% for microcrystalline cellulose to 62.7% for the ball milled cellulose. Accordingly, when using the sulfonated carbon AC-SO_3H, a very high conversion of 82.6% was reached. Glucose, arabinose and HMF were the main products in neat water, while with both the parent AC and the sulfonated AC-SO_3H the product distribution shifted more towards organic acids, i.e. formic, levulinic. lactic, acetic and propionic acid. The carbon balance based on the HPLC data was as high as 73% in the non-catalytic experiment while it dropped to 30% and 60% with AC and AC-SO_3H respectively (Table 2), indicating again as in the case of microcrystalline cellulose the presence of soluble oligomers and the formation of carbonaceous humins. In the case of the two carbons, the conversion based on HPLC data (monomers) was significantly lower compared to that determined either by TOC or by the weight difference method (Table SI-4).

A positive effect on conversion, more pronounced compared to the case of microcrystalline cellulose, was observed by supporting the two metals, i.e. Ru and Pt, on the parent AC, as it increased from 65.3% to 75.2% for 3%Ru/AC-B and 82.8% for 3%Pt/AC-B. As expected, due to the hydrogenating function of these metals, various sugar alcohols were produced with fewer sugars and even less furans and acids (Table 3 and Table SI-5 in the Supporting information). The ruthenium catalyst showed low selectivities, i.e. hexitols (4.1%), C_5 sugar alcohols (5.6%) and glycerol (3.7%), compared to the respective platinum catalyst which exhibited relatively higher selectivity to hexitols (32.4%) followed by glycerol (7.1%) and arabinitol (5.4%). The obvious preference of the 3%Pt/AC-B catalyst for hexitols production can be seen in Fig. 9, where a yield value of 30.1% is obtained compared to the 3.4% for the corresponding 3%Ru/AC-B catalyst.

The combination of Ru or Pt with the acidic sulfonated carbon provided even higher conversion values and selectivity to hexitols (Table 3). When comparing the two metals at the moderate content of 3 wt.%, ruthenium showed a tendency to produce

Table 3
Catalytic results of ball-milled cellulose hydrolytic hydrogenation with Ru and Pt/AC catalysts reduced with $NaBH_4$ (B series) or H_2 at 350 °C (H series) and with bifunctional catalysts (Ru & Pt/AC-SO_3H).

Catalyst	Cellulose conv. (wt.%)	Selectivity (carbon based, % on total converted carbon)								
		C_5–C_6 sugars & cellobiose	Sugar degradation products[a]	Sugar alcohols[b]						
				EG	Gly	C3 diols	C_4	C_5	C_6	Total sugar alcohols
–	62.7	40.7	32.3	–	–	–	–	–	–	–
AC	65.3	3.7	25.8	–	–	–	–	–	–	–
AC-SO_3H	82.6	11.0	48.7	–	–	–	–	–	–	–
3%Ru/AC-B	75.2	5.4	3.0	0.9	3.7	2.1	1.3	5.6	4.1	17.7
3%Pt/AC-B	82.8	3.8	5.9	1.2	7.1	1.8	–	5.4	32.4	47.9
3%Ru/AC-SO_3H	94.8	2.1	1.6	0.8	4.0	1.4	4.5	13.4	41.7	65.8
3%Pt/AC-SO_3H	88.6	1.7	5.6	5.2	3.9	0.4	–	–	49.4	58.9
5%Ru/AC-SO_3H	95.2	1.1	9.9	0.2	7.1	16.7	4.2	3.6	10.2	42.0
5%Pt/AC-SO_3H	96.1	2.2	2.1	0.3	2.3	0.1	0.3	–	64.4	67.4

Reaction conditions: 0.48 g cat., 1.12 g ball-milled cellulose, 2 MPa H_2, 40 mL water, 180 °C, 24 h (2% standard deviation for selectivity values).
[a] Sugar degradation products: HMF, formic acid, levulinic acid, lactic acid, succinic acid, acetic acid, propionic acid, R-OH (aliphatic alcohols, i.e. MeOH, EtOH).
[b] C4 sugar alcohols: sum of threitol and erythritol; C5 sugar alcohols: sum of arabinitol and xylitol; C6 sugar alcohols: sum of sorbitol and mannitol; EG: ethylene glycol; Gly: glycerol; C3 diols: propane-1,2-diol (propylene glycol) and propane-1,3-diol.

more smaller alcohols, such as arabinitol, C4 sugar alcohols, C3 diols (mainly propane-1,2-diol) and glycerol, thus reducing the selectivity towards sorbitol, compared to the platinum catalyst (i.e. C6 sugar alcohols yield of 41.7% with 3 wt.%Ru/AC-SO_3H and 49.4% with 3 wt.%Pt-AC-SO_3H). Previous studies have reported the beneficial use of bifunctional Ru catalysts supported on AC-SO_3H [37] or SiO_2-SO_3H [40], providing high sorbitol yields when using ball milled cellulose, showing also good recyclability and reuse. Although, the 3 wt.% Ru and Pt/AC-SO_3H catalysts of the present study showed appreciable and similar selectivity towards hexitols, increase of the metal loading to 5 wt.% induced a dramatic change in the performance of the Ru catalyst, favoring the production of smaller sugar alcohols (especially of glycerol, propane-1,2-diol and propane-1,3-diol), as can be seen in Tables 3 and SI-5. Such a negative effect on sorbitol yield by increasing Ru loading was also previously observed for the conversion of low crystallinity cellulose over Ru/acidified CNTs catalysts [19]. On the other hand, the 5 wt.%Pt/AC-SO_3H catalyst was even more selective compared to its 3 wt.% analogue and afforded high hexitols yield of 69.5% (at 96.1% conversion) compared to 10.9% (at 95.2% conversion) with the 5 wt.%Ru/AC-SO_3H, as can be seen in Fig. 9.

The carbon balance based on the HPLC data ranged from 26 to 72%, with the bifunctional (Ru or Pt/AC-SO_3H) and those with higher metal loading (5 wt.%) catalysts exhibiting higher values (Table 2). The conversion based on HPLC data (monomers) was significantly lower compared to that determined either by TOC or by the weight difference method (Table SI-4). On the other hand, the conversion values based on TOC data and the weight difference method were similar for the bifunctional and especially for the 5 wt.% metal bifunctional catalysts. All the above indicate that the bifunctional catalysts with metal loading higher than ca. 3 wt.% limit the formation of humins in the hydrolytic hydrogenation of ball-milled cellulose, but the production liquids still contain substantial amounts of soluble oligo-saccharides.

3.5. Catalyst reuse

The ability to reuse the catalyst is very important, especially in batch reactor systems where cellulose (or biomass) and catalyst are mixed together, forming eventually a solid mixture after the reaction, from which it is difficult to recover the solid catalyst, especially in the case of carbon based catalysts that do not allow typical calcination regeneration. In this work, we studied the ability to reuse the most effective catalysts, i.e. 5%Pt/AC-SO_3H and 5%Ru/AC-SO_3H, using the more recalcitrant microcrystalline cellulose as feed. As described in the experimental section, after every run, fresh cellulose was added to the recovered mixture of unconverted cellulose plus catalyst, in order to compensate for the percent of converted cellulose. The respective data for the 5%Pt/AC-SO_3H catalyst are shown in Fig. 10(a).

As it can be seen, the catalyst could be reused for at least 4 runs without reduction of hexitols yield, with the conversion of cellulose exhibiting a progressive increase. This latter observation was attributed to the partial depolymerization of the remaining unconverted cellulose in the solid mixture after every run, which could be hydrolyzed more easily compared to the parent microcrystalline cellulose, thus providing a relatively higher overall degree of conversion in the next run. Similar results were observed for the 5%Ru/AC-SO_3H catalysts, as also shown in Fig. 10(b). Actually, cellulose conversion as well as the yield of hexitols after the first run were both increased to levels similar or even higher than those obtained with the 5%Pt/AC-SO_3H catalyst. The observed good stability in catalytic performance of both catalysts was further supported by the negligible metal leaching, i.e. less than 5 ppb (ICP-AES analysis) of Pt or Ru were detected in the liquid products. The good stability of Ru in similar (i.e. Ru/W/AC catalyst) cellulose hydrogenolysis systems was also previously identified [70]. On the other hand, as can be seen from the data in Table SI-1, significant leaching of S (sulfonic groups) up to ca. 60–80% takes place, under the relatively severe experimental conditions applied (180 °C, 20 bar H_2, 24 h in neat water), in accordance to previous related studies [74]. Nevertheless, it appears that even the remaining acidity of the bifunctional catalysts is sufficient to initiate cellulose hydrolysis for several runs.

3.6. D-Glucose hydrogenation and mechanistic pathways in cellulose hydrolytic hydrogenation

The hydrogenation of glucose has been a reaction of industrial interest for many years due to the potential uses of sorbitol, glycerol, 1,2-propanediol and ethylene glycol (in nutrition, cosmetics, medical and industrial applications). The first applied catalysts have been based on Raney-type nickel (Ni), promoted also with molybdenum (Mo), iron (Fe), chromium (Cr) or tin (Sn). Due to the leaching problems of Ni in the reaction media, its replacement with other catalytic systems, based mainly on supported noble metals, such as ruthenium (Ru), platinum (Pt), palladium (Pd), etc. is being investigated till today [52,75–78]. In the present work, the hydrogenation of glucose was investigated at relatively harsh conditions, as compared to those usually applied, in order to simulate the "one-pot" cellulose hydrolytic hydrogenation system and identify the reaction paths that the in-situ produced glucose undergoes. The

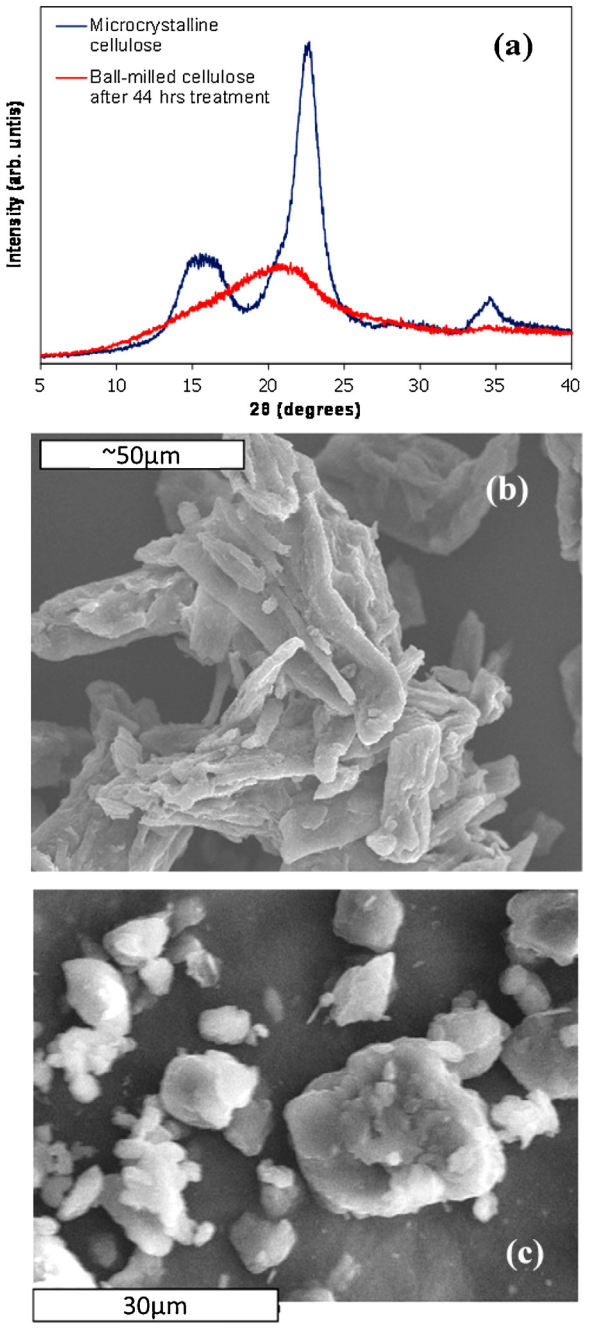

Fig. 8. XRD patterns (a), and SEM images of (b) parent microcrystalline cellulose (Avicel) and (c) Avicel after ball-milling for 44 h.

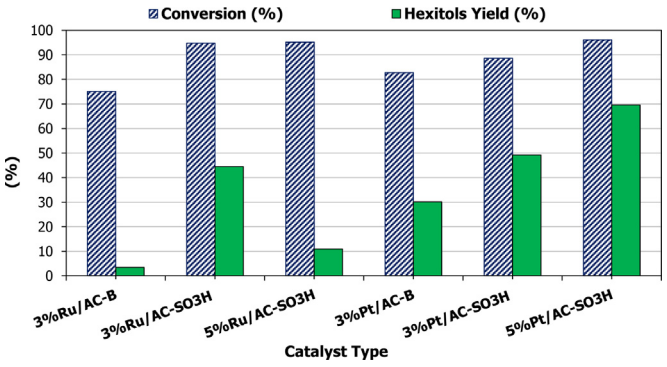

Fig. 9. Conversion (wt.%) of ball-milled cellulose and hexitols yield (wt.%) for the various Ru and Pt/AC supported on parent, non-sulfonated carbon (AC) and on sulfonated carbon (AC-SO_3H) reduced with $NaBH_4$ (reaction conditions: 0.48 g cat., 1.12 g ball-milled cellulose, 2 MPa H_2, 40 mL water, 180 °C, 24 h).

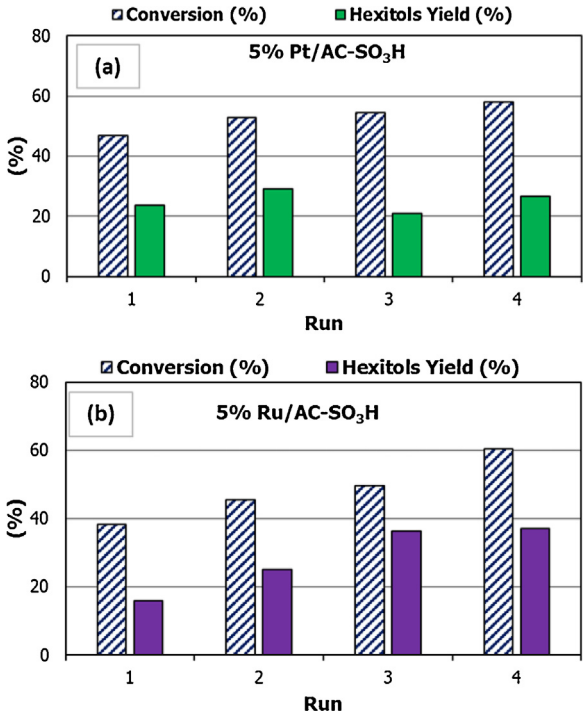

Fig. 10. Conversion (wt.%) of microcrystalline cellulose and hexitols yield (wt.%) with (a) 5%Pt/AC-SO_3H and (b) 5%Ru/AC-SO_3H catalysts for 4 consecutive runs by adding fresh cellulose after each run to compensate for the amount that has been converted.

Pt and Ru/AC catalysts were tested at the relatively high reaction temperature of 180 °C (compared to the 100–120 °C used in most glucose hydrogenation studies with noble metals), for various reaction times (1–24 h) and under the relatively low hydrogen pressure of 2 MPa. All catalysts tested, irrespective of metal loading, type of support (parent AC or sulfonated AC-SO_3H), method of reduction and reaction time, afforded almost 100% conversion of glucose (Table SI-6 in the Supporting information); however, selectivity to hexitols varied depending on the above parameters. In general, when comparing the two metals, it can be clearly seen from the data in Fig. 11 and Table SI-6 that the Pt catalysts supported on either the parent AC or the sulfonated AC-SO_3H carbon, are more selective towards hexitols, especially at prolonged reaction times.

The selectivity to hexitols after 3 h of reaction is 73% and 94% for the 3 wt.%Ru/AC-B and 3 wt.%Pt/AC-B catalysts, respectively (Fig. 11a), and after 24 h it drops to 17% for the ruthenium catalyst, while it remains quite high, at 73%, for the platinum catalyst (Fig. 11b). Furthermore, when the metal loading increases (ca. from 3 to 5%), the formation of hexitols is again clearly favored by the Pt catalysts compared to the Ru ones (Fig. 11a and Table SI-6 in the Supporting information). The above results, mainly those for the 24 h tests, can be directly correlated with the hydrolytic hydrogenation of ball-milled cellulose results (Fig. 9) and can rationalize the observed substantial higher hexitols yield with the 5 wt.%Pt/AC-SO_3H catalyst compared to that with 5 wt.%Ru/AC-SO_3H. On the other hand, less pronounced differences in hexitols yield were found between the Ru and Pt catalysts when the microcrystalline cellulose was used as feed (Fig. 5 and Table 2). This can be attributed to the easier and faster hydrolysis of ball-milled cellulose, thus providing a solution with more abundant glucose, as in the case of glucose hydrogenation tests. Either way, the above data clearly show that the Pt/AC (or Pt/AC-SO_3H) catalysts are more selec-

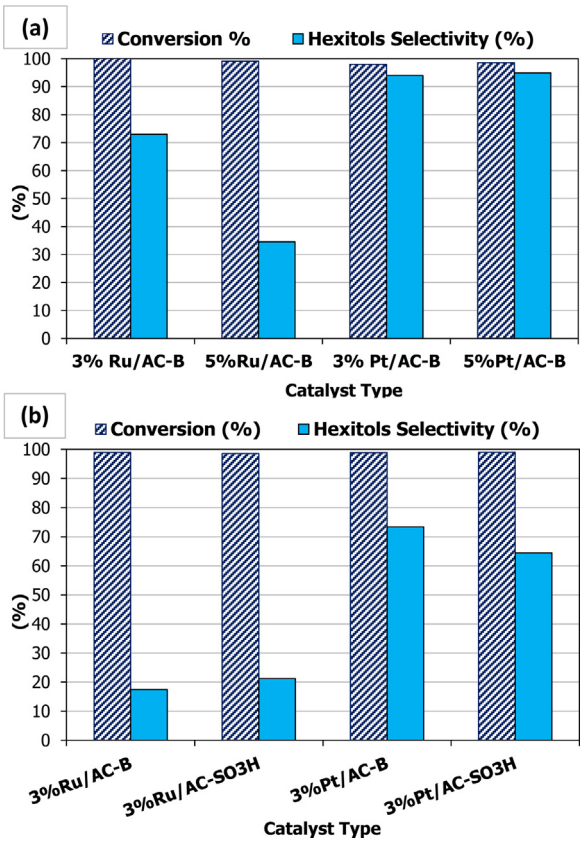

Fig. 11. D-glucose conversion (wt.%) and selectivity to hexitols (%, carbon based on liquids) for the various Ru & Pt/AC catalysts supported on the parent, non-sulfonated carbon (AC) and the sulfonated carbon (AC-SO_3H) that have been reduced with $NaBH_4$ (Reaction conditions: 0.48 g cat., 1.12 g glucose, 2.0 MPa H_2, 40 mL water, 180 °C; time of (a) 3 h and (b) 24 h).

tive towards hexitols compared to the respective Ru catalysts, at relatively low H_2 pressure and harsh conditions, similar to those applied in cellulose hydrolytic hydrogenation.

The scheme in Fig. 12 presents several reaction pathways that have been previously suggested to apply in cellulose hydrolytic hydrogenation [4,22,30,65–70] and are capable to rationalize also the results of the present work. As described in the above paragraph, differences in conversion and selectivity to hexitols and other smaller products were observed in our study depending mainly on three parameters, i.e. the nature of cellulose (microcrystalline or ball-milled amorphous), the type and loading of metal (Pt vs. Ru, 1–5 wt.%), and the nature of the carbon support (parent vs. sulfonated). In the case of microcrystalline cellulose and the parent AC, a strong effect of metal loading, for both metals, can be identified, that is related with the high selectivity of the 1 wt.%Ru and Pt catalysts towards mainly glycerol followed by lower selectivities of C5 (mainly arabinitol) and C4 (mainly threitol) sugar alcohols, propane-1,2-diol, ethylene glycol, as well as hexitols (Table 2). According to the possible reaction pathways of Fig. 12, glycerol can be formed via the direct hydrogenation of glucose to sorbitol (or mannose to mannitol) followed by hydrogenolysis to two molecules of glycerol or via isomerization of glucose to fructose followed by retro-aldol reaction to dihydroxyacetone and glyceraldehyde which are then hydrogenated to glycerol. Taking in consideration the relatively low content of the hydrogenation metal (Pt or Ru) and the basic nature of the parent carbon support (pH of AC-water suspension ~9.5 and pH of the Ru or Pt/AC-water suspension ~5.5–6), the route via isomerization (due to basicity) to fructose followed by retro-aldol reaction (selective retro-aldol C—C cleavage between the α and β position relative to the carbonyl [69]) appears as the most probable. In addition, due to the low metal loading and consequently low hydrogenation activity, the mild acidity offered by the metal or metal oxide phases (identified by the XPS and HRTEM results) as well as by the presence of chlorine "impurities" (as evidenced by XPS and TPD-MS experiments) induced also relatively high selectivity towards propane-1,2-diol via dehydration of glycerol, for both the 1 wt.%Ru and Pt/AC-B catalysts. Furthermore, this mild acidity maybe responsible for the retro-aldol reaction step suggested above.

When the loading of Pt and Ru on the parent AC was increased to 3 and 5 wt.%, selectivity to hexitols (with an average ratio of 50–60% sorbitol and 40–50% mannitol based on ion chromatography measurements) was increased for both metals (Table 2), via the path of direct glucose hydrogenation to sorbitol (Fig. 12), due to the increased hydrogenation function of the catalysts versus their acid function. With respect to the smaller alcohols, increase of metal loading (Pt or Ru) led to lower selectivities, except of arabinitol which remained at the same levels. Interestingly, in the case of Ru catalysts, although the selectivities of the smaller sugar alcohols with the 3 wt.%Ru/AC-B decreased, compared to the 1 wt.%Ru catalyst, they were increased again with the 5 wt.%Ru/AC-B catalyst. This is indicative of a higher hydrogenolysis (C—C cleavage) function of the Ru catalysts, compared to Pt, at least under the relatively low hydrogen pressure conditions and moderate temperature applied in this work. Thus, it can be suggested that at increased metal loadings, especially of Ru, the reaction paths that prevail are the hydrogenation of glucose (or mannose) to sorbitol (or mannitol), followed by its hydrogenolysis mainly to arabinitol, ethylene glycol and glycerol (and propane-1,2-diol via glycerol dehydration), as well as to small aliphatic alcohols (i.e. methanol) (Fig. 12). A third reaction pathway favored by increased Ru loading, that involves the retro-aldol C—C cleavage of glucose towards glycol aldehyde and erythrose, and subsequent hydrogenation of glycol aldehyde to ethylene glycol, may also apply (Fig. 12).

The use of sulfonated carbon (AC-SO_3H) as Pt or Ru support induced similar conversion of microcrystalline cellulose with the catalysts supported on the parent, non-sulfonated carbon (Table 2). This can be attributed to the similar or slightly higher acidity of the former compared to the latter catalysts, as evidenced by Boehm titration and pH measurements (Table 1 and discussion above). However, the selectivity to sorbitol was significantly increased, especially with the higher metal loading catalysts, i.e. the 3 and 5 wt.% Ru or Pt/AC-SO3H catalysts, being similar for the two metals. Furthermore, the total selectivity to sugar alcohols was generally increased with these catalysts (Table 2), thus leading to a better mass balance and carbon efficiency, i.e. the percent of carbon ending up to monomeric sugar alcohols in the liquid product. It appears that the acidity offered by the surface sulfonic groups (–SO_3H) and the $M^o/MOx^{\delta+}$ phases of the catalysts after their treatment with $NaBH_4$ is capable of hydrolyzing cellobiose and other oligo-saccharides initially formed, thus providing more glucose which can then be hydrogenated to sorbitol, according to the reaction paths described above (Fig. 12). The importance of the metal (hydrogenation) versus acidic function of the bifunctional catalysts in cellulose hydrolytic hydrogenation has been also previously discussed in the case of carbon nanofiber-supported nickel catalysts [20]. On the other hand, the total selectivity to sugar alcohols was decreased with the low-metal catalysts. i.e., 1 wt.% Ru or Pt/AC-SO_3H, due to the significant decrease of glycerol selectivity (compared to the 1 wt.%Ru or Pt/AC catalysts) which was not compensated by a substantial increase of sorbitol selectivity. This is an additional indication that the formation of glycerol with the 1 wt.% Ru or Pt/AC catalysts proceeds via glucose isomerization to fructose and subsequent retro-aldol and hydrogenation reactions to glycerol, as discussed above (Fig. 12); the isomerization step is

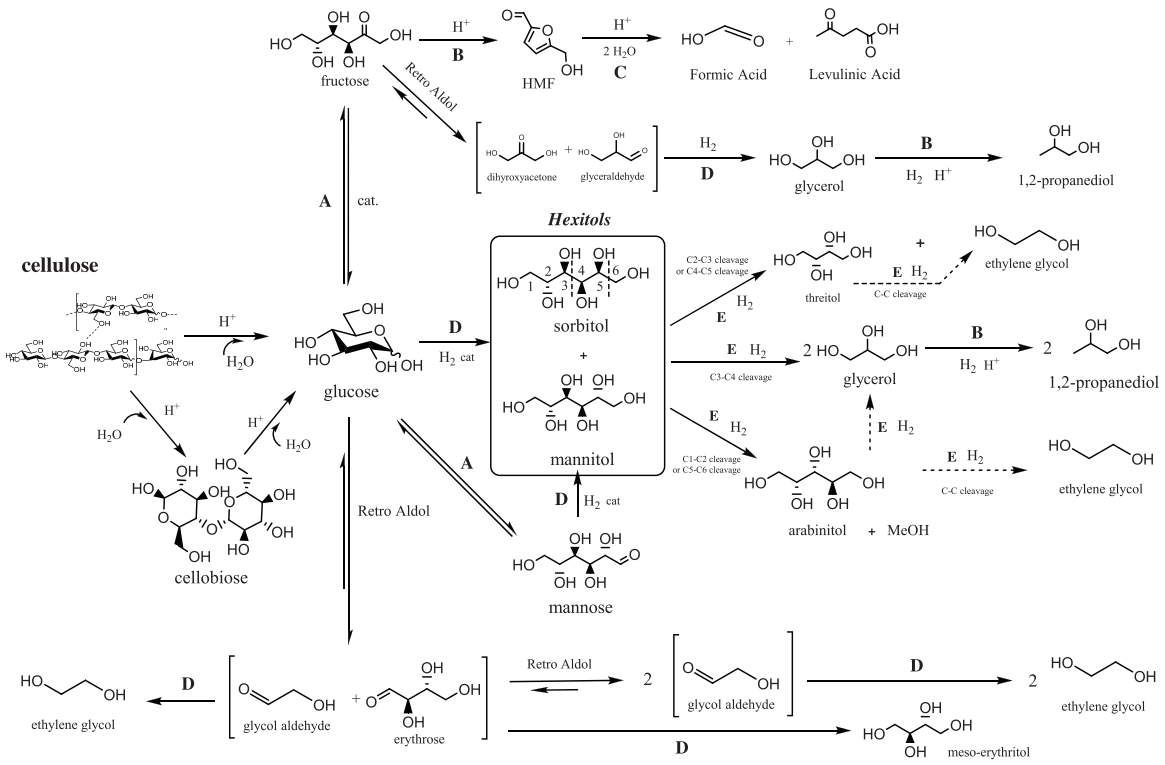

Fig. 12. Main reaction pathways in hydrolytic hydrogenation of cellulose with the various Ru & Pt catalysts supported on micro/mesoporous activated carbon (AC or AC-SO3H) (A): isomerization, (B): dehydration, (C): rehydration, (D): hydrogenation, (E): hydrogenolysis).

favored by the basic parent carbon but it is restricted by the acidic sulfonated carbon support.

When the ball-milled cellulose was used as feed, the total selectivity to sugar alcohols was increased compared to the microcrystalline cellulose, especially with the Pt catalysts (Table 3). This was correlated with the high cellulose conversion (>75%), the higher abundance of monomeric species in the product liquids and the limited formation of humins, mainly with the use of the bifunctional catalysts supported on sulfonated carbon (Table SI-4). The increased total sugar alcohol selectivity with the Pt catalysts on both the parent AC and the sulfonated AC-SO_3H carbons, was due to the increased hexitols selectivity (Table 3). It can thus be suggested that the reaction path that prevails with the Pt catalysts, in sugar-rich aqueous media such as those offered by ball-milled cellulose, is the direct hydrogenation of glucose/mannose to sorbitol/mannitol, accompanied by a relative high stability of the C6 sugar alcohols. On the other hand, although the 3 wt.% Ru catalysts offered a similarly to Pt high hexitols selectivity, the 5 wt.% Ru/AC-SO_3H catalyst exhibited significantly lower hexitols selectivity coupled with higher selectivities to glycerol, propane-1,2-diol, arabinitol, threitol and ethylene glycol, compared to 5 wt.%Pt/AC-SO_3H (Table 3). Such a product distribution can be rationalized with the reaction pathways that involve the direct hydrogenation of glucose/mannose to sorbitol/mannitol followed by enhanced hydrogenolysis (C—C cleavage) to the various smaller sugar alcohols (Fig. 12). This behavior and differences between the two metals supported on either the parent or the sulfonated carbon, was further verified by the glucose hydrogenation experiments conducted under similar experimental conditions (Fig. 11 and related discussion above).

4. Conclusions

The results of the present work showed that cellulose can be effectively converted to valuable sugar alcohols in “one-pot” system at relatively low hydrogen pressure (i.e. 2 MPa) using bifunctional acid-metal catalysts, comprising of highly dispersed Ru or Pt metal/metal oxide phases on micro/mesoporous sulfonated activated carbon. The conversion of cellulose and the yields of sugar alcohols are significantly higher when amorphous, ball-milled cellulose is used. The catalysts were stable for at least 4 consecutive runs; metal leaching was negligible while the substantial removal of sulfonic groups from the sulfonated AC-SO_3H catalysts had a minor effect on their activity and hexitols selectivity. Nevertheless, the most important finding that can offer new insights in the development of efficient catalysts for the hydrolytic hydrogenation of carbohydrates, is the clearly described differences in the performance of Pt and Ru, at least when supported on carbon and at relatively low hydrogen pressure, which is attractive for economical reasons.

Platinum was significantly more selective towards hexitols (sorbitol and mannitol), compared to ruthenium, at relatively high loadings (ca. 3–5 wt.%) which are necessary to promote the hydrogenation of glucose/mannose to sorbitol/mannitol versus other acid-catalyzed reactions, such as retro-aldol which lead to smaller alcohols (as was the case with the 1 wt.%Ru or Pt catalysts, being very selective towards glycerol). On the other hand, ruthenium, afforded high yields of glycerol and propylene glycol (propane-1,2-diol) owing to increased hydrogenolysis (C—C cleavage) of the initially formed hexitols. The above differences in performance were more clearly identified in the case of ball-milled cellulose which can be more easily hydrolyzed to glucose-rich aqueous reaction solutions, compared to the microcrystalline cellulose. Accordingly, similar results were obtained in glucose hydrogenation under the same experimental conditions, as those applied for the hydrolytic hydrogenation of cellulose. Both higher metal loading and longer reaction time (i.e. 24 h) favored the formation of hexitols with the Pt catalysts compared to the corresponding Ru catalysts.

Overall, it was shown that Pt (on activated carbon, sulfonated or not) is more selective towards hexitols compared to Ru, at reaction

conditions required for efficient hydrolysis of cellulose (i.e. 180 °C and 24 h) and at desirable low hydrogen pressures (ca. 2 MPa).

Acknowledgements

K. Triantafyllidis would like to acknowledge co-funding of this research by European Union-European Regional Development Fund and Greek national funds through the Operational program EPAN-II/ESPA 2007-2013/Action "Bilateral Cooperation Greece-Romania" (project 11ROM_8_3_ET 31). V. Parvulescu would like to acknowledge UEFISCDI for the financial support (project PN-II-PCCA-2011-3.2-1367, Nr. 31/2012 and Romania-Greece Joint Research Project Nr. 573/2012). P. Lazaridis would also like to acknowledge the support of COST Action CM0903 for his STSM in University of Bucharest.

Appendix A. Supplementary data

Supplementary data associated with this article can be found, in the online version, at http://dx.doi.org/10.1016/j.apcatb.2017.05.031.

References

[1] R. Parajuli, T. Dalgaard, U. Jørgensen, A.P.S. Adamsen, M.T. Knudsen, M. Birkved, M. Gylling, J.K. Schjørring, Renewable Sustainable Energy Rev. 43 (2015) 244–263.
[2] G.W. Huber, S. Iborra, A. Corma, Chem. Rev. 106 (2006) 4044–4098.
[3] J. Zakzeski, P.C.A. Bruijnincx, A.L. Jongerius, B.M. Weckhuysen, Chem. Rev. 110 (2010) 3552–3599.
[4] J.A. Geboers, S. Van de Vyver, R. Ooms, B. Op de Beeck, P.A. Jacobs, B.F. Sels, Catal. Sci. Technol. 1 (2011) 714–726.
[5] R. Rinaldi, F. Schüth, ChemSusChem 2 (2009) 1096–1107.
[6] Y. Yu, X. Lou, H. Wu, Energy Fuels 22 (2008) 46–60.
[7] D. Yamaguchi, M. Kitano, S. Suganuma, K. Nakajima, H. Kato, M. Hara, J. Phys. Chem. C 113 (2009) 3181–3188.
[8] A. Onda, T. Ochi, K. Yanagisawa, Green Chem. 10 (2008) 1033–1037.
[9] S. Suganuma, K. Nakajima, M. Kitano, D. Yamaguchi, H. Kato, S. Hayashi, M. Hara, J. Am. Chem. Soc. 130 (2008) 12787–12793.
[10] M. Kitano, D. Yamaguchi, S. Suganuma, K. Nakajima, H. Kato, S. Hayashi, M. Hara, Langmuir 25 (2009) 5068–5075.
[11] S. Van de Vyver, J. Geboers, P.A. Jacobs, B.F. Sels, ChemCatChem 3 (2011) 82–94.
[12] M. Grembecka, Eur. Food Res. Technol. 241 (2015) 1–14.
[13] K. Knop, R. Hoogenboom, D. Fischer, U.S. Schubert, Angew. Chem. Int. Ed. 49 (2010) 6288–6308.
[14] A.M. Ruppert, K. Weinberg, R. Palkovits, Angew. Chem. Int. Ed. 51 (2012) 2564–2601.
[15] J.J. Bozell, G.R. Petersen, Green Chem. 12 (2010) 539–554.
[16] N. Li, G.A. Tompsett, T. Zhang, J. Shi, C.E. Wyman, G.W. Huber, Green Chem. 13 (2011) 91–101.
[17] B. Op de Beeck, M. Dusselier, J. Geboers, J. Holsbeek, E. Morre, S. Oswald, L. Giebeler, B.F. Sels, Energy Environ. Sci. 8 (2015) 230–240.
[18] M. Besson, P. Gallezot, C. Pinel, Chem. Rev. 114 (2014) 1827–1870.
[19] W. Deng, X. Tan, W. Fang, Q. Zhang, Y. Wang, Catal. Lett. 133 (2009) 167–174.
[20] S. Van de Vyver, J. Geboers, W. Schutyser, M. Dusselier, P. Eloy, E. Dornez, J.W. Seo, C.M. Courtin, E.M. Gaigneaux, P.A. Jacobs, B.F. Sels, ChemSusChem 5 (2012) 1549–1558.
[21] A. Fukuoka, P.L. Dhepe, Angew. Chem. Int. Ed. 45 (2006) 5161–5163.
[22] H. Kobayashi, Y. Ito, T. Komanoya, Y. Hosaka, P.L. Dhepe, K. Kasai, K. Hara, A. Fukuoka, Green Chem. 13 (2011) 326–333.
[23] H. Kobayashi, Y. Hosaka, K. Hara, B. Feng, Y. Hirosaki, A. Fukuoka, Green Chem. 16 (2014) 637–644.
[24] P. Dhepe, A. Fukuoka, Catal. Surv. Asia 11 (2007) 186–191.
[25] P.L. Dhepe, A. Fukuoka, ChemSusChem 1 (2008) 969–975.
[26] S. Van de Vyver, J. Geboers, M. Dusselier, H. Schepers, T. Vosch, L. Zhang, G. Van Tendeloo, P.A. Jacobs, B.F. Sels, ChemSusChem 3 (2010) 698–701.
[27] R. Palkovits, K. Tajvidi, J. Procelewska, R. Rinaldi, A. Ruppert, Green Chem. 12 (2010) 972–978.
[28] J. Geboers, S. Van de Vyver, K. Carpentier, P. Jacobs, B. Sels, Chem. Commun. 47 (2011) 5590–5592.
[29] S. Liu, Y. Okuyama, M. Tamura, Y. Nakagawa, A. Imai, K. Tomishige, ChemSusChem 8 (2015) 628–635.
[30] J. Geboers, S. Van de Vyver, K. Carpentier, K. de Blochouse, P. Jacobs, B. Sels, Chem. Commun. 46 (2010) 3577–3579.
[31] R. Palkovits, K. Tajvidi, A.M. Ruppert, J. Procelewska, Chem. Commun. 47 (2011) 576–578.
[32] V. Jollet, F. Chambon, F. Rataboul, A. Cabiac, C. Pinel, E. Guillon, N. Essayem, Green Chem. 11 (2009) 2052–2060.
[33] C. Luo, S. Wang, H. Liu, Angew. Chem. Int. Ed. 46 (2007) 7636–7639.
[34] H. Kobayashi, T. Komanoya, K. Hara, A. Fukuoka, ChemSusChem 3 (2010) 440–443.
[35] K.i. Matsumoto, H. Kobayashi, K. Ikeda, T. Komanoya, A. Fukuoka, S. Taguchi, Bioresour. Technol. 102 (2011) 3564–3567.
[36] H. Kobayashi, H. Matsuhashi, T. Komanoya, K. Hara, A. Fukuoka, Chem. Commun. 47 (2011) 2366–2368.
[37] J.W. Han, H. Lee, Catal. Commun. 19 (2012) 115–118.
[38] W. Deng, M. Liu, X. Tan, Q. Zhang, Y. Wang, J. Catal. 271 (2010) 22–32.
[39] F. Chambon, F. Rataboul, C. Pinel, A. Cabiac, E. Guillon, N. Essayem, ChemSusChem 6 (2013) 500–507.
[40] W. Zhu, H. Yang, J. Chen, C. Chen, L. Guo, H. Gan, X. Zhao, Z. Hou, Green Chem. 16 (2014) 1534–1542.
[41] S. Van de Vyver, L. Peng, J. Geboers, H. Schepers, F. de Clippel, C.J. Gommes, B. Goderis, P.A. Jacobs, B.F. Sels, Green Chem. 12 (2010) 1560–1563.
[42] G. Liang, H. Cheng, W. Li, L. He, Y. Yu, F. Zhao, Green Chem. 14 (2012) 2146–2149.
[43] G. Liang, L. He, H. Cheng, W. Li, X. Li, C. Zhang, Y. Yu, F. Zhao, J. Catal. 309 (2014) 468–476.
[44] H. Wang, J. Lv, X. Zhu, X. Liu, J. Han, Q. Ge, Top. Catal. 58 (2015) 623–632.
[45] A. Negoi, K. Triantafyllidis, V.I. Parvulescu, S.M. Coman, Catal. Today 223 (2014) 122–128.
[46] R.M. Ravenelle, F. Schüβler, A. D'Amico, N. Danilina, J.A. van Bokhoven, J.A. Lercher, C.W. Jones, C. Sievers, J. Phys. Chem. C 114 (2010) 19582–19595.
[47] D.K. Mishra, A.A. Dabbawala, J.J. Park, S.H. Jhung, J.-S. Hwang, Catal. Today 232 (2014) 99–107.
[48] T. Ennaert, J. Van Aelst, J. Dijkmans, R. De Clercq, W. Schutyser, M. Dusselier, D. Verboekend, B.F. Sels, Chem. Soc. Rev. 45 (2016) 584–611.
[49] T. Ennaert, J. Geboers, E. Gobechiya, C.M. Courtin, M. Kurttepeli, K. Houthoofd, C.E.A. Kirschhock, P.C.M.M. Magusin, S. Bals, P.A. Jacobs, B.F. Sels, ACS Catal. 5 (2015) 754–768.
[50] J. Hilgert, N. Meine, R. Rinaldi, F. Schuth, Energy Environ. Sci. 6 (2013) 92–96.
[51] T. Kilpiö, A. Aho, D. Murzin, T. Salmi, Ind. Eng. Chem. Res. 52 (2013) 7690–7703.
[52] P.A. Lazaridis, S. Karakoulia, A. Delimitis, S.M. Coman, V.I. Parvulescu, K.S. Triantafyllidis, Catal. Today 257 (Part 2) (2015) 281–290.
[53] A. Aho, S. Roggan, O.A. Simakova, T. Salmi, D.Y. Murzin, Catal. Today 241 (Part B) (2015) 195–199.
[54] M. Besson, P. Gallezot, A. Perrard, C. Pinel, Catal. Today 102–103 (2005) 160–165.
[55] D.Y. Murzin, E.V. Murzina, A. Tokarev, N.D. Shcherban, J. Wärnå, T. Salmi, Catal. Today 257 (Part 2) (2015) 169–176.
[56] I.L. Simakova, Y.S. Demidova, E.V. Murzina, A. Aho, D.Y. Murzin, Catal. Lett. 146 (2016) 1291–1299.
[57] F. Auneau, M. Berchu, G. Aubert, C. Pinel, M. Besson, D. Todaro, M. Bernardi, T. Ponsetti, R. Di Felice, Catal. Today 234 (2014) 100–106.
[58] M. Yabushita, H. Kobayashi, A. Fukuoka, Appl. Catal. B: Environ. 145 (2014) 1–9.
[59] Q.-Y. Liu, Y.-H. Liao, T.-J. Wang, C.-L. Cai, Q. Zhang, N. Tsubaki, L.-L. Ma, Ind. Eng. Chem. Res. 53 (2014) 12655–12664.
[60] J. Chen, S. Wang, J. Huang, L. Chen, L. Ma, X. Huang, ChemSusChem 6 (2013) 1545–1555.
[61] J. Xi, Y. Zhang, Q. Xia, X. Liu, J. Ren, G. Lu, Y. Wang, Appl. Catal. A: Gen. 459 (2013) 52–58.
[62] N. Meine, R. Rinaldi, F. Schüth, ChemSusChem 5 (2012) 1449–1454.
[63] S.L. Goertzen, K.D. Thériault, A.M. Oickle, A.C. Tarasuk, H.A. Andreas, Carbon 48 (2010) 1252–1261.
[64] Y.S. Kim, S.J. Yang, H.J. Lim, T. Kim, C.R. Park, Carbon 50 (2012) 3315–3323.
[65] T. Soták, T. Schmidt, M. Hronec, Appl. Catal. A: Gen. 459 (2013) 26–33.
[66] H. Li, D. Yu, Y. Hu, P. Sun, J. Xia, H. Huang, Carbon 48 (2010) 4547–4555.
[67] B. Op de Beeck, J. Geboers, S. Van de Vyver, J. Van Lishout, J. Snelders, W.J.J. Huijgen, C.M. Courtin, P.A. Jacobs, B.F. Sels, ChemSusChem 6 (2013) 199–208.
[68] X. Wang, L. Meng, F. Wu, Y. Jiang, L. Wang, X. Mu, Green Chem. 14 (2012) 758–765.
[69] R. Ooms, M. Dusselier, J.A. Geboers, B. Op de Beeck, R. Verhaeven, E. Gobechiya, J.A. Martens, A. Redl, B.F. Sels, Green Chem. 16 (2014) 695–707.
[70] K. Fabicovicova, M. Lucas, P. Claus, Green Chem. 17 (2015) 3075–3083.
[71] R. Weingarten, W.C. Conner, G.W. Huber, Energy Environ. Sci. 5 (2012) 7559–7574.
[72] G. Tsilomelekis, M.J. Orella, Z. Lin, Z. Cheng, W. Zheng, V. Nikolakis, D.G. Vlachos, Green Chem. 18 (2016) 1983–1993.
[73] Y. Ogasawara, S. Itagaki, K. Yamaguchi, N. Mizuno, ChemSusChem 4 (2011) 519–525.
[74] A.H. Van Pelt, O.A. Simakova, S.M. Schimming, J.L. Ewbank, G.S. Foo, E.A. Pidko, E.J.M. Hensen, C. Sievers, Carbon 77 (2014) 143–154.
[75] P. Gallezot, P.J. Cerino, B. Blanc, G. Flèche, P. Fuertes, J. Catal. 146 (1994) 93–102.
[76] P. Gallezot, N. Nicolaus, G. Flèche, P. Fuertes, A. Perrard, J. Catal. 180 (1998) 51–55.
[77] B.W. Hoffer, E. Crezee, P.R.M. Mooijman, A.D. van Langeveld, F. Kapteijn, J.A. Moulijn, Catal. Today 79–80 (2003) 35–41.
[78] B. Kusserow, S. Schimpf, P. Claus, Adv. Synth. Catal. 345 (2003) 289–299.